Modeling surface temperature under clouds using geo-stationary satellite observations

Lei Lu
March, 2009

Course Title:	Geo-Information Science and Earth Observation for Environmental Modelling and Management
Level:	Master of Science (Msc)
Course Duration:	September 2007 - March 2009
Consortium partners:	University of Southampton (UK) Lund University (Sweden) University of Warsaw (Poland) International Institute for Geo-Information Science and Earth Observation (ITC) (The Netherlands)
GEM thesis number:	2007-xx

Modeling surface temperature under clouds using geo-stationary satellite observations

by

Lei Lu

Thesis submitted to the International Institute for Geo-information Science and Earth Observation in partial fulfilment of the requirements for the degree of Master of Science in Geo-information Science and Earth Observation for Environmental Modelling and Management

Thesis Assessment Board

Chair person:	Prof. Andrew Skidmore
Internal examiner:	Dr. A.S.M. Ambro Gieske
External Examiner	Prof. Terry Dawson
Supervisor:	Mr. Valentijn Venus

ITC International Institute for Geo-Information Science and Earth Observation
Enschede, The Netherlands

Disclaimer

This document describes work undertaken as part of a programme of study at the International Institute for Geo-information Science and Earth Observation. All views and opinions expressed therein remain the sole responsibility of the author, and do not necessarily represent those of the institute.

Abstract

Land surface temperature (LST) has a high impact on energy exchanges between surface and atmosphere, climate change, and climatic and hydrological modelling. However, clouds make it difficult to obtain LST from satellite observations of thermal infrared bands directly. The application in polar-orbiting satellite observations proved that the neighboring-pixel approach (NP) based on surface energy balance (SEB) is potential in retrieval of LST under clouds. This study utilized the method to geostationary satellite data MSG/SEVIRI to obtain LST under clouds with high temporal resolution which is more close to the dynamic weather. The four-channel algorithm was used to retrieve LST under clear skies, and the Heliosat-2 algorithm was applied to estimate solar irradiance. Both Navasha, Kenya and Burkina Faso were taken as study areas and *in situ* data from these areas were used for validation. The RMSE of LST under clear skies was 4.5 K for Naivasha and 5.55 K for Burkina Faso in daytime, and the RMSE of estimated solar irradiance was 234.05 Wm^{-2}.for Naivasha, 388.414 Wm^{-2} for Burkina Faso. However, error derived from estimating LST under clear skies contributed more to the accuracy of estimated LST under clouds (RMSE=5.6 K for Naivasha). Both temporal interpolation and spatial interpolation were applied to interpolate LST under clouds by using neighboring-pixel approach, and the temporal interpolation performed best (RMSE=5.6 K for temporal interpolation, RMSE=20.14K for spatial interpolation, RMSE=11.76 K for a combination of the previous two methods). This indicates that the neighboring-pixel approach is sensitive to heterogeneity of land surface, and temporal interpolation can eliminate the effect of heterogeneity of land surface. The statistic analysis on LST under clouds shows that the hypothesis “there is no difference between estimated LST under clouds from satellite observations and *in situ* data” was rejected at the level of 0.05. Using neighboring-pixel approach based on SEB, LST under clouds in daytime was obtained; in order to obtain the diurnal LST in all skies, method for estimating LST under clouds in nighttime is necessary.

Acknowledgements

With starting the acknowledgement, I know the GEM MSc course really comes to the end. It is so hard to find words to express my appreciations to the organizations and people who have helped me during the 18 months, but I would like to take this opportunity to use simple words to describe my deepest gratitude.

First of all, many thanks to Erasmus Mundus-GEM MSc course, and its organizers-the staff from Southampton University, Lund University, Warsaw University and ITC, as well as Prof. Geping Luo who introduced this course to me. During the past 18 months, I have not only learnt knowledge from teachers, but made many good friends and learnt lots of things from them as well. This experience has been branded in my life forever.

I would like to express my sincere appreciate to Mr. Valentijn Venus. Thank you very much to spend your time on numerous occasions to discuss with me about research issues, study problems during my study, as well as your great help in the fieldwork. I am also very grateful for Prof. Andrew Skidmore. Thank you for the valuable suggestions to the thesis and encouragement to me when I was depressed by the work. I thank Dr. Jan de Leeuw, Dr. A.G. (Bert) Toxopeus, Dr. Ir.C.A.J.M. (Kees) de Bie, Mr. Andre Kooiman and Mr. Willem Nieuwenhuis. Thank all of you for your great ideas, contributions, and invaluable guidance throughout my study period.

Especial gratitude goes to Dr. Jörg Szarzynski from University of Bonn, Dr. Robert Becht from ITC and your work team for your helps in data sharing. Thank also goes to Mr. Murat Ucer for your effort in fixing instruments for my field work.

Many thanks to Mr. Tiejun Wang and Ms. Yali Si. I got so much happiness and encouragements from you. Thank you to give me great help in my life and my study in Netherland.

I would like to thank all of my GEM classmates. All of you were the most important part of my fantastic life in the past 18 months. From UK to Sweden, from Poland to the Netherlands, we met each other, knew each other, got used to each other, shared so much happiness with each other. I can not image the scene when we leave, it is so hard to say goodbye. Dear GEM students, I love you all and hope we are good friends forever.

Last but not least, I would like to thank my parents and people of the big family as well as friends in China, for your love and support forever.

Table of contents

List of figures

List of tables

Acronym

ADAS	Automatic Data Acquisition System
ASTER	Advanced Spaceborne Thermal Emission and Reflection Radiometer
AVHRR	Advanced Very High Resolution Radiometer
ETM+	Enhanced Thematic Mapper Plus
FAO	Food and Agricultural Organization
GCM	General Circulation model
GOES	Geostationary Operational Environmental Satellite
HRV	High Resolution Visible
IDV	Integrated Data Viewer
ISCCP	International Satellite Cloud Climatology Project
LOWTRAN	Low Altitude Atmospheric Transmission
LSE	Land Surface Emissivity
LST (T_s)	Land Surface Temperature
MODIS	Moderate Resolution Imaging Spectroradiometer
MODTRAN	Moderate Resolution Atmospheric Radiance and Transmittance Model
MSG	Meteosat Second Generation
NP	Neighboring-pixel approach
RTE	Radiative Transfer Equation
SEB	Surface Energy Balance
SEVIRI	Spinning Enhanced Visible and Infrared Imager
SSI	Surface Solar Irridiance
Stvd.	Standard Deviation
RMSE	Root Mean Square Error
F_n	Net Long wave Radiation
S_n	Net Solar Radiation
R_n	Net Radiation
G	Soil Heat Flux
H	Sensible Heat Flux
LE	Latent Heat Flux

$S\downarrow$	Incoming Shortwave Radiation
$S\uparrow$	Upwelling Shortwave Radiation
$F\downarrow$	Downwelling Longwave Radiation
$F\uparrow$	Upwelling Longwave Radiation
$S_0\downarrow$	Clear Sky Solar Radiation
T_d	Sublayer Temperature of Soil
T_a	Air Temperature
$T_{s-clear}$	Land Surface Temperature in Clear Skies
$T_{s-cloud}$	Land Surface Temperature under clouds
p	Reflectance
Tl	Linke Turbidity Factor

1. Introduction

1.1. Background

Land surface temperature (LST) affects the mass, energy and momentum exchanges between land and atmosphere. It is generally referred as surface skin temperature which is inferred from the thermal emission of the earth surface measured by a radiometer based on Plank's law. Traditionally, it is approximated from standard surface air temperature (T_a) measured by a sheltered thermometer 1.5-3.5 meters above a flat and well-ventilated surface. Although surface skin temperature is highly correlated with surface-air temperature, they are different (Lakshmi et al., 1998; Jin et al., 1997). Compared with surface air temperature, surface skin temperature relates to surface properties more directly, and is important for understanding many terrestrial biogeophysical precesses (Jin et al., 1997). In this research, land surface temperature (T_s) mentioned means the surface skin temperature instead of surface air temperature.

Land surface temperature is an important land surface parameter which is indispensable for a wide range of applications, such as interpreting global warming (Jin and Dickinson, 2002), study in numerical atmospheric models like general circulation models (GCMs) (McNider et al., 1994), niche mapping for reptile (Kearney and Porter, 2004), soil moisture estimation (Wang et al., 2007), environmental monitoring, surface energy balance (SEB) (Chchbouni et al., 1993), evapotranspiration and crop yield prediction (Mallick et al., 2007;Guo and Cheng, 2004). Also, the forecasts of numerical weather prediction models can be improved by use of accurate fields of surface fluxes and soil moisture which depend on LST (Deneke et al., 2008).

Information about surface temperature on different spatial and temporal scales, together with air temperature and soil moisture are important for modeling and monitoring latent and sensible heat fluxes in the biophysical

processes, as well as the potential relationship between land surface energy budget and hydrological budget. In the energy balance equation, the net radiation derived from net solar radiation and net longwave radiation is partitioned as soil heat flux, sensible heat flux and latent heat flux. The sensible heat flux is the flow of energy as a result of the temperature gradient between surface temperature and air temperature. Therefore, surface temperature is an important input parameter for calculating sensible heat flux, and also significant in the evapotranspiration determination as an application of the principle of the energy balance.

Weather and climate determined by surface temperature, air temperature and motions of the atmosphere and oceans are driven by energy exchanges. During this process, clouds play an important role in regulating the earth radiation budget (Smith et al., 2004). Clouds cover more than half of the globe at a given time and influence radiative energy exchanges which mainly includes albedo effect (increase of reflected solar radiation with increasing cloudiness) and greenhouse effect (decrease of emitted longwave radiation with increasing cloudiness) (Heffter et al., 1995).

At global scale, global mean cloud cover and surface temperature are not independent (Paltridge, 1974). On average, the presence of clouds is associated with a cooler surface (Groisman et al., 2000). Aiguo Dai et al. (1999) considered the changes in cloud cover as one of the causes for decreasing of diurnal range of surface air temperature worldwide during the last 4-5 decades. However, surface temperature has high correlation with surface air temperature; furthermore, quantitative analysis of the relationship between surface temperature and properties of cloud cover, further the feedback for the climate change and hydrological cycle. This makes estimating surface temperature under clouds a significant field in remote sensing. Spatially distributed land surface temperature data including surface temperature with cloudiness in high temporal resolution are desired for several modeling applications (Venus and Rugege, 2008; Schneider et al., 1978). However, a literature review shows that there are few studies that target the retrieval of land surface temperature under clouds by using satellite observations.

1.2. Research problem and justification

In spite of its high accuracy as well as no limitation under cloudy conditions, ground based measurements with a thermal radiometer can not provide information about the spatio-temporal pattern of surface temperature. Using satellite measurements in the thermal infrared becomes popular since satellites estimate surface temperature with uniform and different spatial and temporal scales, and make it possible for environmental monitoring, modeling and prediction in different spatio-temporal scales.

Under cloudy conditions, it is difficult to retrieve the surface temperature directly from satellite observations because of the absorption of the clouds. Generally, remote sensors in thermal infrared bands record the radiation related to the cloud top temperature for cloudy pixels, this can not give the correct information from land surface. Therefore, in research estimating surface temperature under clouds, it is common to utilize surface temperature in clear sky or surface air temperature obtained from weather station as a reference (Jin, 2000; Minnis and Harrison, 1984). Though there is correlation between surface temperature and air temperature, differences exist, especially for the daytime when the difference is up to over 10 K (Stisen et al., 2007).

As early as 1980s, research on LST under clouds by using nearby pixels, time interpolation and the relationship between air temperature and surface temperature was first undertaken (Minnis and Hrrison, 1984; Minnis et al. 1990). However, these methods only tested small areas without considering the influences of surface vegetation and soil properties on temperature. Key and Wong (1999) proposed an empirical algorithm for estimating LST in cloudy sky, which was applied to sea ice that its feasibility on land surface with complicated land cover is unknown. By parameterization of net longwave radiation and sensible and latent heat fluxes into net solar radiation, Jin (2000) proposed a neighboring-pixel approach to estimate LST of cloudy pixels from polar-orbiting satellite observations, the basic concept of which is the similarity of surface properties between cloudy pixels and

their neighboring pixels. However, weather and climate are dynamic and always changing over a wide range of time scales, and a gap of radiation budget measurements would be caused if only polar-orbiting satellite observations are used (Smith, 2004). The latest research related to retrieval of LST under clouds was performed by Aires et al. (2004) in the study to obtain global surface temperature diurnal cycle over land under clear and cloudy conditions with temporal interpolation of 3-hourly surface skin temperature that was estimated by the ISCCP from the infrared measurements collected by the polar and geostationary satellites, in which the microwave satellite data were used to provide information of the surface under clouds. Microwave signals can penetrate clouds, and with satellite microwave observations, surface temperature in cloudy conditions can be estimated (Aires et al, 2004). At present, passive microwave satellite measurements are only collected from polar orbits. This limits the number of overpasses per day at a given location.

With a temporal resolution as high as 15 minutes, MSG/SEVIRI data offer continuous observations about land surface and provide useful information about variation of clouds and surface temperature. A broadband ranging from 0.4 to 11 μm makes it convenient to estimate solar radiation as well.

In this study, the neighboring-pixel approach based on SEB will be attempted to apply to retrieve LST under clouds from MSG/SEVIRI observations, in which an approach for estimating solar radiation of all sky named Heliosat-2 will be explored. Strategies for interpolation of LST under clouds using neighboring-pixel approach will also be explored. The approach will be tested and validated on data collected in Lake Naivasha, Kenya by ITC, NRS&WRS departments and data about Burkina Faso.

1.3. Research objectives

1.3.1. General objective

The general objective of this research is to model land surface temperature under clouds by using geostationary satellite data.

1.3.2. Specific objectives

To achieve the general objective, three steps are necessary to be implemented according to the concept of the neighboring-pixel approach based on SEB. They are described as following:

(a) To estimate at least five days of diurnal land surface temperature under clear skies from the satellite data
(b) To obtain the incoming solar radiation (solar irradiance) corresponding to the period of surface temperature in (a)
(c) To interpolate the surface temperature under clouds with the surface temperature under clear skies, with incoming solar radiation

1.4. Research questions

To achieve the specific objectives listed above, the following research questions must be answered:

(a) What is the accuracy of the estimated LST under clear skies from the satellite data?
(b) What is the accuracy of the estimated solar irradiation from the satellite data?
(c) Is the accuracy of LST under clouds produced in this study higher than the LST of cloudy pixels estimated with polar-orbiting satellite observations?

1.5. Research hypotheses

According to the specific objectives in this research, there are three hypotheses for testing aiming to the three models, including the four-channel model for retrieval of LST in clear sky, Heliosat-2 model for estimating solar irradiance, and the method for estimating LST under clouds. Comparing with the *in situ* observations, the hypotheses testing in this research should determine if each model yields biased estimates. Therefore, the hypotheses can be given as following:

(a) For four-channel algorithm to retrieve the LST under clear skies

H_0: There is no difference between estimated LST from the four-channel algorithm and observed LST

Ha: There is difference between estimated LST from the four-channel algorithm and observed LST

(b) For Heliosat-2 algorithm to estimate solar irradiance

H_0: There is no difference between estimated solar irradiance from Heliosat-2 and observed solar irradiance

Ha: There is difference between estimated solar irradiance from Heliosat-2 and observed solar irradiance

(c) For LST under clouds derived from the method proposed in this research

H_0: There is no difference between estimated LST under clouds and observed LST under clouds

Ha: There is difference between estimated LST under clouds and observed LST under clouds

1.6. Outline of the thesis

Chapter 2: describes and summarizes the literature with respect to the present research in retrieval of LST, solar radiation as well as basic environmental physics needed to understand the research topic

Chapter 3: Generally describes the characteristics of data used in this study including satellite data and *in situ* data, principle and framework of the

general methodology of this study, and the algorithms used to achieve the final objective.

Chapter 4: Presents the results derived from models, validation of models and hypothesis testing.

Chapter 5: Discusses the implication from the results

Chapter 6: Concludes the findings of this study, and give some recommendations and opportunities for further research.

2. Literature Review

2.1. Effects of atmosphere on LST

To retrieve LST from the satellite observations which are recorded as spectral radiance, there are two major obstacles referring to emissivity and atmospheric effects. The conversion of brightness temperatures to thermodynamic temperatures requires emissivity of the surface, which is influenced by soil moisture significantly as well as soil type, land cover and land use (Sun and Pinker, 2004). The absence of emissivity measurements makes it difficult to obtain LST (Timmermans et al., 2008). In addition to the radiances from clouds, the effects of atmosphere on LST mainly come from water vapour in the 10.5-12.5 μm window region, in which the typical values of water vapour transmittance vary from 95 percent for dry atmospheres to 30-40 percent for wet atmospheres (Caselles et al., 1997). Furthermore, the influence of other atmospheric constituents including fixed gases and aerosols can not be neglected. MODTRAN and LOWTRAN models are used for atmospheric correction in retrieval of LST, as well as split-window, triple-channel, four-channel algorithms which use simultaneous measurements in different infrared channels to achieve the atmospheric correction. However, these methods can not remove the effects of clouds.

Haze refers to small particles from both natural sources and anthropogenic sources dispersed throughout the atmospheric aerosol in polluted areas. Its particles consist of tiny salt crystals, exceedingly fine dust, or products of combustion, with radius varying up to 0.5 μm. These fine particles scatter and absorb solar radiation, and also act as cloud condensation nuclei so that it influences the optical properties of clouds. The fine particles typically reside in the atmosphere for days to weeks, and they can be transported over thousands of kilometers before disappearance. With appropriate meteorological conditions, the area affected by haze can extend over 10^6 square kilometers or more (Chameides, 1999). As an example, in the south

Asian region which is characterized by a monsoonal climate, a haze layer can be identified every dry monsoon season over most of the North Indian Ocean and the South/Southeast Asian continent since the beginning of the INDOEX campaign in 1995 (Chung et al., 2002). In general, the attenuation of haze in visible bands is more than the reduction of infrared radiation because of the smallness of the haze particles (Chen, 1975). It mainly redistributes the solar radiation between the surface and the atmosphere (Chung et al., 2002).

On average, cloudy-sky conditions represent more than half of the actual day-to-day weather (Jin, 2000). For radiative balance of the earth, clouds decrease the surface temperature by reflecting solar radiation, and absorb thermal radiation emitting from the surface and emit it at a lower temperature which increase the surface temperature (Jin et al., 1996). It has been demonstrated that clouds combining with secondary damping effects from soil moisture and precipitation can reduce diurnal range of surface air temperature by 25%-50% (Dai, 1999). According to Dai (1999), the diurnal range of surface air temperature had decreased worldwide during the last 4-5 decades and the changes in cloud cover were cited as one of the likely causes. Therefore, the similar effect can be expected in LST due to the close relationship between surface air temperature and LST (Jin, 2000, Stisen et al., 2007). On average, clouds decrease the net radiative heating of the earth except cirrus clouds which increase the net radiative heating of the earth if they are optically thin enough. As early as 1978, researchers have performed the studies in which cloudiness was referred as a climatic feedback mechanism (Schneider et al., 1978), and a warm surface temperature perturbation would cause the increase of cloudiness. Therefore, a continuous time satellite observations including overcast moments on LST is essential in environmental studies and climate modeling.

2.2. Models to estimate LST

LST varies spatially according to soil type, soil moisture, land use and land cover, and temporally with the time of day and season of the year. As a result, conventional ground-based observations of LST are not representative

of large areas. In the last decades, several approaches have been published for retrieval of LST from satellite data. According to the radiometric channels used for retrieving LST, there are single-channel algorithms which include the one based on radiative transfer equation (RTE) with a main constraint of need of *in situ* radiosounding launched simultaneously with the satellite passes, Qin et al.'s (2001) mono-window algorithm that avoids the limitation in RTE method and developed the algorithm with atmospheric water vapor and near-surface air temperature, and a generalized single-channel method developed by Jiménez-Muñoz and Sobrino who only used the atmospheric water vapor content (Jiménez-Muñoz and Sobrino, 2003); split-window algorithms with a basic principle of taking advantage of difference of absorption of water vapour in two adjacent spectral windows (usually are 10.5-11.5 μm and 11.5-12.5 μm) to correct atmospheric effects, within which the surface temperature is described as a linear combination of brightness temperature measured in both thermal channels(Sobrino et al., 1994; Yang and Yang, 2006), and multiple-band algorithms like triple-window algorithm and four channel algorithm in which the mid-infrared channels are added for atmospheric correction, LST in both daytime and nighttime is estimated.

To determine accurate values of LST, knowledge of land surface emissivity (LSE) is required because natural surface do not act as blackbodies. However, the temperature and emissivity can not be calculated simultaneously since the number of unknown variables is always higher than the number of measurements. For a sensor with N spectral channels, N equations can be established in which there are always N+1 unknowns including N spectral emissivities and the surface temperature. To overcome this problem, a priori information is needed, and different techniques have been developed including the reference channel method, the emissivity normalization method (Valor et al., 2003), the temperature spectral indices method (Becker and Li, 1990), the spectral ratio method, the alpha derived emissivity method, the gray body method, the classification-based emissivity method (Peres and DaCamara, 2005), the temperature emissivity separation method (Goïta and Royer, 1997) and vegetation cover method (Peres and DaCamara, 2004).

With these algorithms, LST with different spatial and temporal scales can be estimated from different satellite observations. Most of these studies focus on the clear sky situations which means the values about LST are derived from the pixels without clouds. Polar-orbiting satellites located at a height between 700 km and 800 km above the surface provide surface information with high spatial resolution, for example, 90 m for ASTER TIR scanner, 120 m for thermal band of Landsat data, and 1 km for thermal bands of MODIS and AVHRR data. However, the temporal resolution of polar-orbiting satellites is not as high as geostationary satellites which scan a given site with an interval of 3 hours for GOES, and 15 minutes for SEVIRI aboard Meteosat second generation satellites. Landsat satellites revisit a given site about 16 days; MODIS observations can be obtained twice a day because both of Terra and Aqua satellites carry the MODIS sensors. Though spatial resolution of geostationary satellite observations is lower than polar-orbiting satellites, time sequence of observations is essential in this study to obtain LST under clouds.

2.3. Relation between LST and surface energy balance

With exception of net solar radiation, other terms in surface energy balance (SEB) are related to LST.

The energy from the sun and emission of atmosphere must be equal to the energy leaving the land surface simultaneously. This process can be expressed with the following equation:

$$R_n = G + LE + H \qquad (1)$$

where G is soil heat flux (Wm^{-2}), LE is latent heat flux (Wm^{-2}), H is sensible heat flux (Wm^{-2}), R_n is the net radiation (Wm^{-2}) which can be also written as:

$$R_n = S_n - F_n \qquad (2)$$

in which S_n (Wm^{-2}) is net solar radiation that is the difference of incoming solar radiation minus upward solar radiation reflected by the surface. F_n is net longwave radiation (Wm^{-2}) referred as the difference between incoming longwave radiation and outgoing longwave radiation, which depend on air temperature and LST, respectively. In FAO 56, net longwave radiation is computed as (Nandagiri and Kovoor, 2005)

$$F_n = \sigma\left(\frac{T_{\max}^4 + T_{\min}^4}{2}\right)(0.34 - 0.14\sqrt{e_a})(1.35\frac{S\downarrow}{S_0\downarrow} - 0.35) \qquad (3)$$

Where σ is Stephan-Boltzmann constant; $T_{\max}$ and $T_{\min}$ are maximum and minimum air temperature, respectively; e_a is actual vapor pressure; $\frac{S\downarrow}{S_0\downarrow}$ is the relative shortwave radiation, and $S_0\downarrow$ is clear sky solar radiation.

Soil heat flux (G) reflects the heat exchange between surface and sublayer of soil, which has positive correlation with temperature gradient, thermal capacity and thermal conductivity. On the basis of the conventional force-restore method (Jin 2000; Deardorff, 1978; Dickinson, 1988), it can be written as:

$$G = k_g \frac{\partial T}{\partial Z} = k_g \frac{(T_s - T_d)}{\Delta Z} \qquad (4)$$

k_g is thermal molecular conductivity of ground soil in units $Wm^{-1}K^{-1}$, T_d is sublayer temperature, T_s is land surface temperature, and ΔZ is the depth of subsurface layer.

Sensible heat flux (H) denotes the heat exchange between land surface and the turbulent boundary layer. It is usually written as (Chehbouni et al., 1993),

$$H = \rho C_p \frac{(T_s - T_a)}{r_{ac}} \quad (5)$$

where ρ is the air density (kg/m^3), C_p is the air specific heat at constant pressure (J/kg·°C), T_a is air temperature, r_{ac} is the aerodynamic resistance (s/m).

Latent heat flux (LE) is the total amount of water evapotranspired by vegetation and evaporated from the soil, which is always referred as evapotranspiration. There are different models for calculating LE, including Hargreaves method, Turc radiation method, Makkink radiation method, and the Penman-Monteith method which is written as (Monteith, 1965; Jacobs et al., 2004; Nandagiri and Kovoor, 2005),

$$LE = \frac{0.408\Delta(R_n - G) + \gamma \frac{37}{T_{ahr} + 273} u(e^0(T_{ahr}) - e_a)}{\Delta + \gamma(1 + 0.34u)} \quad (6)$$

Where:

R_n net radiation at the grass surface [MJ m^{-2} hour^{-1}]

G soil heat flux [MJ m^{-2} hour^{-1}]

T_{ahr} mean hourly air temperature [˚C]

Δ saturation slope vapour pressure curve at T_{ahr} [kPa˚C^{-1}]

γ psychometric constant [kPa˚C^{-1}]

$e^0(T_{ahr})$ saturation vapour pressure at air temperature T_{ahr} [kPa]

e_a average hourly actual vapour pressure [kPa]

u average hourly wind speed [m/s]

3. Materials and methods

3.1. General description of data

3.1.1. Description of satellite data

This research utilized digital data with an interval of 15 minutes from the Meteosat Second Generation (MSG) satellite (from Meteosat-8 onwards) Spinning Enhanced Visible and Infrared Imager (SEVIRI) from June 2008. Meteosat-8 which was the first MSG satellite launched in August 2002 is located over 0° latitude and 3.4ºW longitude with a nominal coverage including the whole of Europe, all of Africa and locations at which the elevation to the satellite is greater than or equal to 10°. The imaging sampling distance is 1 km for the High Resolution Visible (HRV) channel, and 3 km at the sub-satellite point for other 11 standard channels. Table 1 shows a summary of the main features about these 12 spectral channels. With these 12 spectral channels, SEVIRI possesses unique capabilities for cloud imaging and tracking, fog detection, measurement of the Earth-surface and cloud-top temperature, tracking of ozone patterns as well as many other improved measurements.

Table 1 Spectral characteristics of SEVIRI channels (EUMETSAT,2008)

Channel number	Channels	Nominal central wavelength (μm)	Spectral Band (μm)
1	Visible band 0.6	0.635	0.56-0.71
2	Visible band 0.8	0.81	0.74-0.88

3	Near-infrared band 1.6	1.64	1.50-1.78
4	Infrared band 3.9	3.92	3.48-4.36
5	Water vapour band 6.2	6.25	5.35-7.15
6	Water vapour band 7.3	7.35	6.85-7.85
7	Infrared band 8.7	8.70	8.30-9.10
8	Ozone band 9.7	9.66	9.38-9.94
9	Infrared band 10.8	10.8	9.80-11.80
10	Infrared band 12.0	12.0	11.00-13.00
11	Carbon Dioxide band 13.4	13.40	12.40-14.40
12	Broadband high-resolution visible band		0.4-11

In this research, the reflectance derived from the HRV band was used to estimate the global irradiance by using the Heliosat-2 algorithm. The brightness temperature from IR3.9, IR8.7, IR11 and IR12 was used to drive the model for estimating land surface temperature under clear skies, which is named as four-channel algorithm. Additionally, the brightness temperature of IR3.9, IR8.7, IR11, IR12 and IR13 was utilized for cloud layer mask. The details about the algorithms mentioned above will be described in the following sections.

3.1.2. Ground data

The ground data used for parameterisation and validation in this project were received from an Automatic Acquisiton System (ADAS) station in Naivasha (0º16’40” S, 36º29’03” E), Kenya performed by NRS and WRS Departments, ITC. Another dataset about Burkina Faso (11°09’42.2” N, 03°04’34.1” W) from Biophysical Observation Network in West Africa was used as well. In the dataset of Naivasha, all the parameters including land surface temperature, air temperature, solar radiation were measured with an interval of 15 minutes between October 2007 and September 2008. In addition, wind speed, relative humidity and pressure were measured with which the net long wave radiation and evapotranspiration (also referred as latent heat flux) that were parameterized into net solar radiation based on the surface energy balance in this research. Parameters including land surface

temperature, air temperature, downwelling solar radiation, upwelling solar radiation, downwelling longwave radiation and upwelling longwave radiation in Burkina Faso were measured with intervals of both 15 minutes and 10 minutes in 2005.

For the final objective of this study, the surface temperature under clouds was estimated by using the neighboring-pixel approach on the basis of SEB (surface energy balance). The relative terms in SEB must be known, including net solar radiation, net long-wave radiation, sensible heat flux and latent heat flux. However, it is difficult to measure these items directly. The way to obtain them is to calculate indirectly by using other parameters which can be measured. Net solar radiation (S_n) was calculated as $(1-0.23)*S\downarrow$ where $S\downarrow$ is incoming solar radiation, namely solar irradiance, and 0.23 is albedo referring to the surface reflection coefficient in Naivasha. Net long-wave radiation (F_n) which is the difference between incoming and outgoing long wave radiation is expressed as (Nandagiri and Kovoor, 2005):

$$F_n = \sigma\left(\frac{T_{\max}^4 + T_{\min}^4}{2}\right)(0.34 - 0.14\sqrt{e_a})(1.35\frac{S\downarrow}{S_0\downarrow} - 0.35) \quad (1)$$

Where σ is Stephan-Boltzmann constant; $T_{\max}$ and $T_{\min}$ are maximum and minimum air temperature, respectively; e_a is actual vapor pressure; $\frac{S\downarrow}{S_0\downarrow}$ is the relative shortwave radiation, and $S_0\downarrow$ is clear sky solar radiation. According to FAO 56, $\frac{S\downarrow}{S_0\downarrow}$ ranges from 0.7 to 0.8 for arid and semi arid areas, hence a value of 0.75 was used for the relative solar radiation here.

The latent heat flux (LE), namely evaportranspiration, was calculated in Excel by Wangmo who used the famous Penman-Monteith equation standardized by the Food Agriculture Organization (FAO) (Nandagiri and

Kovoor, 2005). In this procedure, the grass reference surface was assumed to be 12 cm in height with a surface resistance of 70s/m and an albedo of 0.23.

$$LE = \frac{0.408\Delta(R_n - G) + \gamma \frac{37}{T_{ahr} + 273} u(e^0(T_{ahr}) - e_a)}{\Delta + \gamma(1 + 0.34u)} \qquad (2)$$

Where

R_n net radiation at the grass surface [MJ m^{-2} $hour^{-1}$]

G soil heat flux [MJ m^{-2} $hour^{-1}$]

T_{ahr} mean hourly air temperature [˚C]

Δ saturation slope vapour pressure curve at T_{ahr} [kPa˚C^{-1}]

γ psychometric constant [kPa˚C^{-1}]

$e^0(T_{ahr})$ saturation vapour pressure at air temperature T_{ahr} [kPa]

e_a average hourly actual vapour pressure [kPa]

u average hourly wind speed [m/s]

All the parameters above about the weather information were available in time series.

3.2. General methodology for estimation of land surface temperature (LST) under clouds

The retrieval of LST under clouds using neighboring-pixel approach is derived from the SEB principle under the assumption that the surface radiation amount and balance are dependent on the sky condition. In other words, it is assumed that the net effect of clouds on surface radiation includes a decrease in surface insolation and an increase in downward longwave radiation, though the magnitude of this net effect is controversial at the global scale.

The surface radiative balance can be expressed as (Jin 2000):

$$R_n = S_n - F_n \quad (3)$$

where RN is the net radiation of land surface, S_n is net solar radiation which can be calculated as (Jacobs et al., 2004):

$$S_n = S\downarrow - S\uparrow = (1-\alpha)S\downarrow \quad (4)$$

$S\downarrow$ is incoming shortwave radiation from the sun, $S\uparrow$ is the upwelling shortwave radiation reflected by the surface, α is the albedo.

F_n in (1) is net longwave radiation, which is derived from (Jacobs et al., 2004):

$$F_n = F\downarrow - F\uparrow = \varepsilon_a \sigma T_a^4 - \varepsilon_s \sigma T_s^4 \quad (5)$$

where $F\downarrow$ is downwelling longwave radiation from atmosphere, which can be calculated by using $\varepsilon_a \sigma T_a^4$, ε_a is effective emissivity of the atmosphere, T_a is air temperature; $F\uparrow$ is upwelling longwave radiation emitted by land surface, which is expressed as $\varepsilon_s \sigma T_s^4$, ε_s is land surface emissivity, T_s is surface temperature. σ is Stefan-Baltzman constant.

In surface energy balance, the net radiation can also be expressed as (Chehbouni et al., 1993)

$$R_n = G + H + LE \quad (6)$$

where G is soil heat flux, , H is sensible heat flux, LE is latent heat flux.
Soil heat flux can be described as (Jin 2000):

$$G = k_g \frac{\partial T}{\partial Z} = k_g \frac{(T_s - T_d)}{\Delta Z} \quad (7)$$

k_g is thermal molecular conductivity of ground soil in units $Wm^{-1}K^{-1}$, T_d is sublayer temperature, and ΔZ is the depth of subsurface layer.
Combining equation (3) and (6), there is

$$G = S_n - F_n - H - LE \qquad (8)$$

In equation (8), the terms of G, F_n, H and LE are related to air temperature and surface temperature. Considering H and LE as one term expressed as S_{hle}, equation (8) can be made partial difference to surface temperature T_s mathematically as (Jin 2000) :

$$\frac{\partial G}{\partial T_s} = \frac{\partial S_n}{\partial T_s} - \frac{\partial F_n}{\partial T_s} - \frac{\partial S_{hle}}{\partial T_s} \qquad (9)$$

It has been observed that the sublayer temperature T_d is much less sensitive to surface insolation than the LST, thus, there is (Jin 2000)

$$\frac{\partial G}{\partial T_s} = \frac{\partial}{\partial T_s}\left[k_g \frac{(T_s - T_d)}{\Delta Z}\right] \approx \frac{k_g}{\Delta Z} \qquad (10)$$

In addition (Jin 2000),

$$\frac{\partial S_{hle}}{\partial T_s} \approx \frac{\Delta S_{hle}}{\Delta T_s} = \frac{\Delta S_{hle}}{\Delta S_n}\frac{\Delta S_n}{\Delta T_s} \qquad (11)$$

$$\frac{\partial F_n}{\partial T_s} \approx \frac{\Delta F_n}{\Delta T_s} = \frac{\Delta F_n}{\Delta S_n}\frac{\Delta S_n}{\Delta T_s} \qquad (12)$$

ΔF_n, ΔS_{hle} and ΔS_n can be approximated as difference of net longwave radiation F_n between cloudy pixel and its neighboring pixel under clear

skies, difference of $(H+LE)$ between cloudy pixel and its neighboring pixel under clear skies, and difference of net solar radiation S_n between cloudy pixel and its neighboring pixel under clear skies. Though S_{hle} and F_n are the terms related to surface temperature, in this study surface temperature T_s was the parameter that we estimated as the research objective. It has been reported (Jin 2000) that linear relationship between net longwave radiation and net solar radiation, and $(H+LE)$ (also S_{hle}) and net solar radiation, namely

$$F_n = aS_n + a_0 \quad (13)$$

$$S_{hle} = bS_n + b_0 \quad (14)$$

The coefficients a and b depend on surface type. Combining the equation (9)-(14), there is (Jin 2000)

$$\Delta T_s = \frac{1}{\lambda}(1-a-b)\Delta S_n = \frac{1}{K}\Delta S_n \quad (15)$$

ΔT_s is considered as the difference of surface temperature between cloudy pixel $T_{s-cloud}$ and pixel under clear skies $T_{s-clear}$. λ denotes $\frac{k_g}{\Delta Z}$, and $\frac{1}{K} = \frac{1-a-b}{\lambda}$.

According to equation (15), the surface temperature under clouds $T_{s-cloud}$ can be interpolated from surface temperature under clear skies $T_{s-clear}$. We explored three ways for interpolation in this study, including temporal interpolation, spatial interpolation, and combined interpolation which is a hybrid of temporal interpolation and spatial interpolation.

For temporal interpolation, the $T_{s-cloud}$ is expressed as

$$T_{s-cloud}(t,i) = T_{s-clear}(t-1,i) + \frac{1}{K}[S_n(t,i) - S_n(t-1,i)] \qquad (16)$$

in which i means the number of the pixel, $T_{s-cloud}(t,i)$ denotes the surface temperature of pixel i at the time of t which is under clouds. $T_{s-clear}(t-1,i)$ denotes the surface temperature of pixel i is under clear skies at the time of $(t-1)$. Correspondingly, $S_n(t,i)$ means the net solar radiation of pixel i at the time of t; $S_n(t-1,i)$ denotes the net solar radiation of pixel i at the time of $(t-1)$. If the pixel was covered by clouds at next time $(t+1)$, $T_{s-cloud}(t+1,i)$ was retrieved using equation (16), however, $T_{s-clear}(t-1,i)$ was changed into LST under clouds derived at last time, namely $T_{s-cloud}(t,i)$. Therefore, the time iteration was formed to obtain LST under clouds if the clouds covered the pixel for couple of hours or even longer time.

For spatial interpolation, $T_{s-cloud}$ is expressed as

$$T_{s-cloud}(t,i) = \frac{1}{n}\sum_j \{T_{s-clear}(t,j) + \frac{1}{K}[S_n(t,i) - S_n(t,j)]\} \qquad (17)$$

where $T_{s-cloud}(t,i)$ is the surface temperature of pixel i at the time of t which is under clouds; $T_{s-clear}(t,j)$ is the surface temperature of pixel j at the time of t, j is the number of neighboring pixels of pixel i, and these neighboring pixels were selected with a window of 3×3 pixels in which the pixel i was located in the center of the window. Correspondingly, $S_n(t,i)$ is the net solar radiation of pixel i at the time of t, and $S_n(t,j)$ is the net solar radiation of pixel j. n is the number of neighboring pixels under clear skies.

The third interpolation strategy is the combination of temporal interpolation and spatial interpolation. For this method, the neighboring pixels of the cloudy pixel were searched at first. If there was no neighboring pixel under

clear skies, the temporal interpolation was adopted; otherwise, the spatial interpolation was utilized.

A four-channel algorithm was used for retrieval of LST under clear skies, and the Heliosat-2 algorithm was utilized for estimating solar irradiance. The framework of this study is shown in Fig. 1.

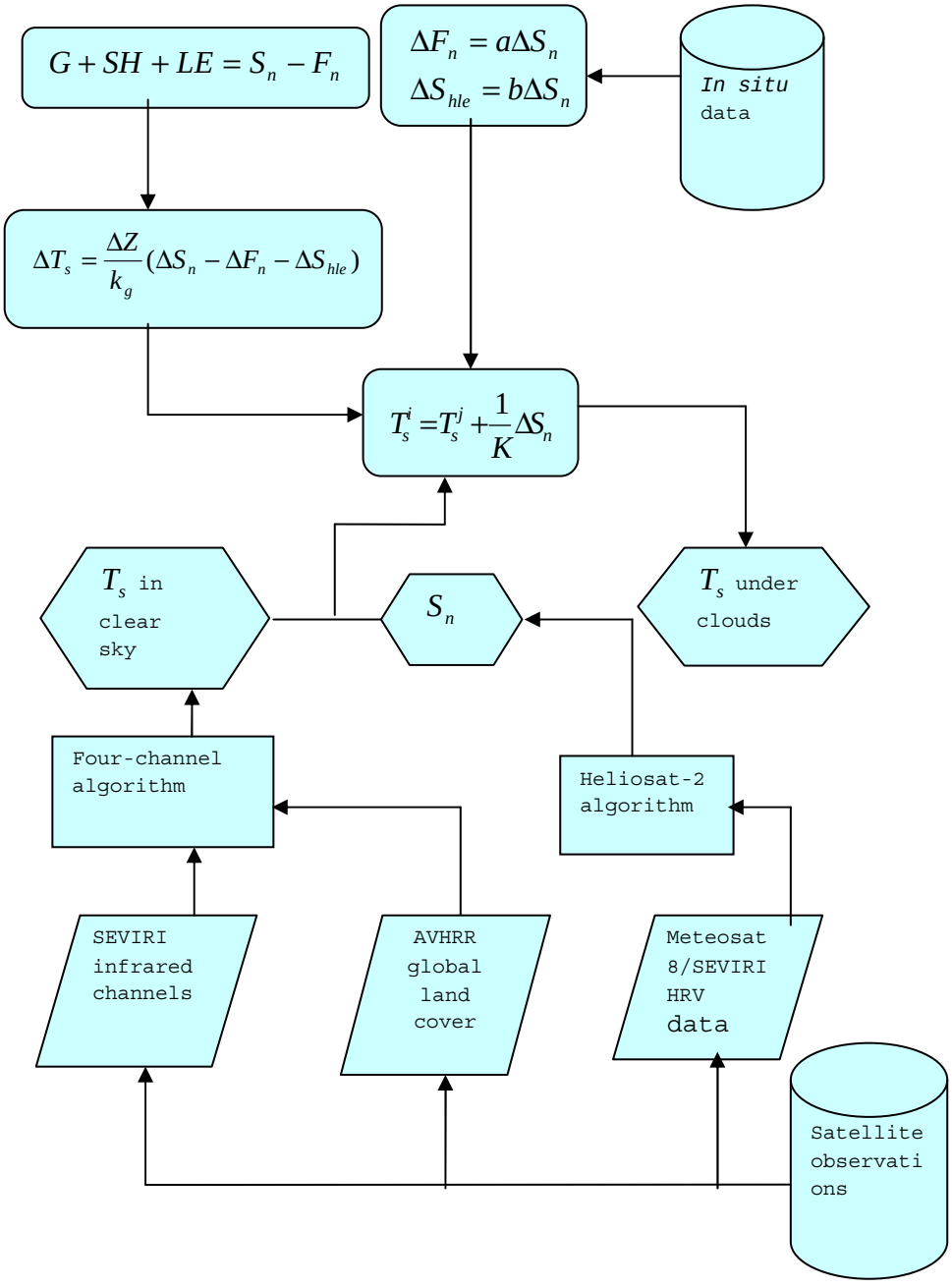

Fig. 1 Framework for estimating LST under clouds

3.3. Methodology for estimation of global irradiance

Solar irradiance, one of the components of solar radiation, is referred as surface insolation, which indicates the amount of downwelling solar energy incident on a horizontal surface and integrated over the total solar spectrum.

Heliosat-2 is the algorithm used to estimate the surface solar irradiance from geostationary satellite observations, especially for the Meteosat Secondary Generation satellites. It overcomes the drawback of other algorithms which contain biases because of 3D radiative effects from the variability of clouds, and the sun and satellite geometries. This algorithm takes these geometries into account by parameterizing the ground reflectance as a function of the angle between the directions to the sun and satellite as seen from ground, which is the so called co-scattering angle. The 3D radiative effects are considered in both the inversion step of estimating cloud properties and the forward model for predicting the surface solar irradiance.

In this algorithm, there is a key parameter named cloud index "n", which derives from a comparison of radiance observed by the sensor to the one observed over the corresponding pixel when the sky is clear related to the clearness of the atmosphere. Briefly, the cloud index n could be considered as the description of attenuation of the atmosphere. The cloud index n is expressed mathematically as (Dagestad and Olseth, 2005):

$$n^t(i,j) = \frac{p^t(i,j) - p^t{}_g(i,j)}{p^t{}_{cloud} - p^t{}_g(i,j)} \qquad (18)$$

Where

$p^t(i,j)$ is the reflectance, or apparent albedo that observed by the satellite sensor for the time t and the pixel (i,j)

$p^t{}_{cloud}(i,j)$ is the reflectance over the brightest clouds

$p^t{}_g(i,j)$ is the reflectance over the ground under clear sky.

If the sky is clear, the reflectance $p^t(i, j)$ is close to the one of the ground and the cloud index n is close to 0 (possibly negative). If the sky is overcast, the cloud index n is close to 1 (or larger).

For $p^t{}_g(i, j)$, a polynomial of co-scattering angle has been given by Dagestad and Olseth (2005) based on the data about six sites. In this research, the third order polynomial of co-scattering angle fitted to 15 percentiles within each ten degree bin (total 12 bins) was applied to calculate $p^t{}_g(i, j)$. The reflectance over the brightest clouds $p^t{}_{cloud}(i, j)$ was derived from the 98 percentile of the counts of the pixels according to Dagestad's suggestion, which was assumed to be the reflectance of the "thickest clouds".

The global irradiance was calculated using the empirical relationship mentioned in Dagestad and Olseth's research (2005) with the cloud index n as input:

$$\begin{aligned} k &= 1.2 && \text{if } n < -0.2 \\ k &= 1 - n && \text{if } n \in [-0.2, 0.8] \\ k &= 2.0667 - 3.6667n + 1.6667n^2 && \text{if } n \in [0.8, 1.1] \\ k &= 0.05 && \text{if } n > 1.1 \end{aligned} \qquad (19)$$

Where k is the clear sky index which is defined as the ratio of the actual global irradiance $S\downarrow$ to the clear sky global irradiance $S_0\downarrow$ (Dagestad and Olseth, 2005),

$$k = \frac{S\downarrow}{S_0\downarrow} \qquad (20)$$

The clear sky global irradiance, $S_0\downarrow$, is calculated as the sum of the direct $S_d\downarrow$ and diffuse $S_{df}\downarrow$ horizontal irradiations under clear sky with the Linke turbidity factor Tl (Lefèvre et al., 2002).

$$S_0\downarrow = S_d\downarrow \times \cos(\theta_s) + S_{df}\downarrow \quad (21)$$

where θ_s is solar zenith angle,

$$S_d\downarrow = 1367 \times E_0 \times \exp(-0.8662 \times Tl \times r_0 \times ms) \quad (22)$$

$$S_{df}\downarrow = 1367 \times {E_0}^2 \times \cos(\theta_s) \times [0.0065 + (-0.045 + 0.0646 \times Tl) \times \cos(\theta_s) + (0.014 - 0.0327 \times Tl) \times (\cos\theta_s)^2] \quad (23)$$

where E_0 is eccentricity correction factor, Tl is the Linke turbidity factor (Lefèvre et al., 2002),

$$Tl = \frac{1}{r_0 \times ms} \times \lg[1367/(1367 \times E_0 \times \cos\theta_s)] \quad (24)$$

r_0 is Rayleigh optical thickness and ms is air mass which expresses the ratio of the optical path length of the solar direct irradiance through the atmosphere to the optical path through a standard atmosphere at sea level with the sun at the zenith (Lefèvre et al., 2002),

$$ms = 0.9669/[\cos(\theta_s) + 0.50572 \times (96.07995 - \theta_s)^{-1.6364}] \quad (25)$$

If $ms < 20$

$$r_0 = 1/(6.6296 + 1.7513 \times ms - 0.1202 \times ms^2 + 0.0065 \times ms^3 - 0.00013 \times ms^4)$$

If $ms > 20$ $r_0 = 1/(10.4 + 0.718 \times ms)$

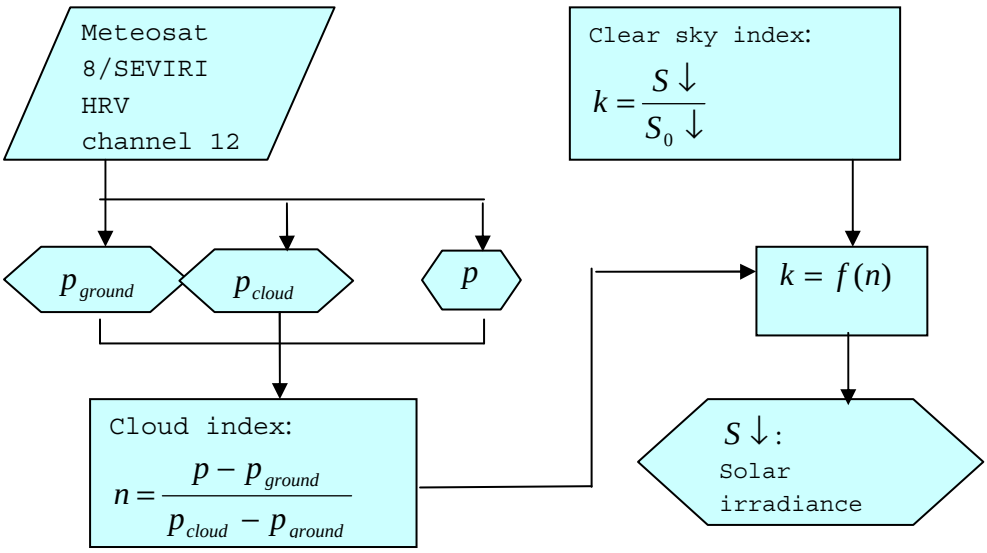

Fig. 2 Framework for estimating solar irradiance

3.4. Methodology for estimation of land surface temperature in clear sky

Accurate retrieval of surface temperature under clouds with neighboring-pixel (NP) approach requires good estimates of the surface temperature of a given scene in the absence of cloud cover since the basic assumption is that presence of clouds in the sensor field of the view alters the clear-sky temperature. Therefore, considerable effort is devoted to the clear-sky surface temperature. Clear-sky temperature is the measured or modeled temperature of a cloud-free scene (Minnis and Harrison, 1984).

Based on the radiative transfer model and the characteristics of channels in infrared of MSG SEVIRI data, Sun et al. (2007) proposed a four-channel algorithm in which the LST in clear sky is the combination of the four thermal window channels including 3.9 μm, 8.7 μm, 11 μm and 12 μm, and the surface emissivity is calculated according to a linear mixing with weighted sum of land cover percentage times the emissivity of corresponding surface type. The land cover data used as parameterization of surface emissivity were generated with a global AVHRR data at 8-km

resolution, which includes 14 International Geosphere-Biosphere Programme (IGBP) land cover classes. Because of the contribution of the solar radiation reflected by the earth surface in 3.9 μm mid-infrared channel, the radiative transfer models are a little different between daytime and nighttime. The retrieval of LST derived from the four-channel algorithm is divided into LST in daytime and nighttime, respectively.

For nighttime, the retrieval of LST in clear sky is expressed as (Sun et al. 2007):

$$T_s(l) = a_0(l) + a_1(l)T_{11} + a_2(l)(T_{11} - T_{12}) + a_3(l)(T_{3.9} - T_{8.7}) + a_4(l)(T_{11} - T_{12})^2 + a_5(l)(\sec\theta - 1) \qquad (26)$$

where

l is the surface type index which ranges from 1 to 14; θ is the viewing angle; T_{11}, T_{12}, $T_{3.9}$ and $T_{8.7}$ are the brightness temperatures of corresponding channels as the subscript numbers; T_s is the retrieved LST in clear sky. a_0, a_1, a_2, a_3, a_4, a_5 are empirical coefficients shown in Table 2.

Table 2 Coefficients for the four-channel nighttime algorithm (Sun et al., 2007)

Surface type index (l)	a_0	a_1	a_2	a_3	a_4	a_5
1	-22.8035	1.0884	1.8823	0.3357	0.2987	350.8949
2	-22.7543	1.0907	1.8862	0.4184	0.3198	363.5047
3	-3.837	1.0068	-1.4470	-0.1766	0.4803	5.2194
4	0.2181	1.0468	-0.8622	2.3312	0.3009	265.9501
5	32.3526	0.9289	-3.0455	2.3989	2.0019	129.5428
6	-24.8056	1.1165	1.2838	1.0085	0.0132	405.8485
7	-26.4230	1.1073	1.5419	0.6305	0.2045	394.3541
8	-14.0548	-10.054	1.6736	-0.4148	0.3697	260.4226
9	-24.7400	1.0971	2.5880	-0.1936	0.7697	316.1983

10	-24.0435	1.0934	1.9820	0.1464	0.5767	323.6190
11	-22.7214	1.0873	1.6851	0.1604	0.9131	267.3659
12	-23.6807	1.0943	1.3240	0.4622	0.6197	253.8679
13	-21.1784	1.0844	2.0485	0.1141	0.3397	342.6013

For daytime, the retrieved LST in clear sky is expressed as (Sun et al., 2007):

$$T_s(l) = a_0(l) + a_1(l)T_{11} + a_2(l)(T_{11} - T_{12}) + a_3(l)(T_{3.9} - T_{8.7}) + a_4(l)(T_{11} - T_{12})^2 + a_5(l)(\sec\theta - 1) + a_6(l)T_{3.9}\cos\theta_s \quad (27)$$

where l is the surface type index; θ is the viewing angle; θ_s is solar zenith angle; T_{11}, T_{12}, $T_{3.9}$ and $T_{8.7}$ are the brightness temperatures of corresponding channels as the subscript numbers; T_s is the retrieved LST in clear sky; a_0, a_1, a_2, a_3, a_4, a_5 , a_6 are empirical coefficients shown in Table 3. θ is the viewing angle; θ_s is solar zenith angle.

Table 3 Coefficients for the four-channel daytime algorithm (Sun et al., 2007)

Surface type index (l)	a_0	a_1	a_2	a_3	a_4	a_5	a_6
1	-22.0814	1.0814	2.2893	0.1548	0.2231	405.7598	-0.00001
2	-20.3907	1.0719	2.6695	-0.0192	0.3732	406.9285	-0.00006
3	-26.2765	1.0955	2.2214	-0.1240	0.8902	331.8644	-0.00007
4	4.1951	2.2883	-1.4199	4.1236	0.5705	221.0204	-1.2434
5	-21.8708	1.0772	2.4627	-0.0364	0.5027	398.2049	0.00057
6	-24.2113	1.0872	2.8053	0.1559	-0.0113	448.2403	0.00088
7	-24.8435	1.0888	2.6812	-0.0241	0.2563	446.4928	0.00006
8	-13.0879	1.0645	0.7628	-0.0060	0.0932	246.8655	0.00039
9	-23.5439	1.0955	2.0301	-0.0384	0.2725	323.6286	0.0005
10	-23.9135	1.0891	2.3913	-0.0300	0.6885	337.0811	0.00033
11	-23.0139	1.0839	2.3772	-0.0620	0.7999	335.4042	0.00007
12	-21.9462	1.0776	2.6429	0.0044	0.5170	340.9291	-0.00007
13	-19.0341	1.0726	2.2138	-0.0075	0.3460	343.9272	0.00027

3.5. Estimation of LST under clouds

In addition to retrieving LST under clear skies and solar irradiance with the methods described above, another three parameters are necessary to know in order to achieve the final objective of this study. They are the coefficients between net solar radiation and net longwave radiation, net solar radiation and sensible and latent heat fluxes, and soil conductivity. The net solar radiation is the difference between solar irradiance and reflected soalr irradiance. If the albedo α of the surface is known, net solar radiation can be determined by $S_n = (1-\alpha)S\downarrow$. In this study, the albedo of the surface in Naivasha is 0.23, and 0.16 for Burkina Faso. Using *in situ* data with respect to radiation, the linear relationship between net solar radiation and sensible and latent heat fluxes, and net solar radiation and net longwave radiation is shown in Fig. 3, respectively. Corresponding to the general methodology, the coefficients for parameterized net longwave radiation and sensible-latent heat fluxes are 0.0004 and 0.8996 for Naivasha, 0.1851 and 0.7277 for Burkina Faso, respectively. In addition to these coefficients, the parameter K in neighboring-pixel approach depends on soil thermal conductivity (k_g) as well. Peters-Lidard et al. (1998) listed the thermal properties of soil constituents according to Farouki's research as Table 4. In Jin's (2000) research, the soil and ground properties for different soil types, even with composition of moisture and mineral, were presented. As the specific soil properties were unknown in this study, the soil thermal conductivity was estimated indirectly by using the estimates of ground heat flux which is assumed as 10 percent of net radiation, which is based on the principle that the soil thermal conductivity affects the land surface energy balance through its role in calculating the ground heat flux. It is expressed as (Peters-Lidard et al., 1998),

$$G = (k\frac{\partial T}{\partial z})\Big|_{z=0} \qquad (28)$$

As a result, the soil thermal conductivity was estimated as 2.86 W m^{-1} K^{-1} in Naivasha, and 1.18 W m^{-1} K^{-1} in Burkina Faso. Therefore, the parameter K was 286 W m^{-2} K^{-1} and 135.32 W m^{-2} K^{-1} in the two areas.

Table 4 Thermal properties of soil constituents (Peters-Lidard, 1998)

Material	Density (×103kgm^{-3})	Specific heat (J kg^{-1} K^{-1})	Heat capacity (×103 J K^{-1} m^{-3})	Thermal conductivity (W m^{-1} K^{-1})
Quartz	2.65	733	1942	8.4
Soil minerals	2.65	733	1942	2.9
Soil organics	1.30	1926	2503	0.25
Water	1.00	4186	4186	0.6
Ice	0.90	2093	1883	2.5
Air	0.0012	1005	1.20	0.026

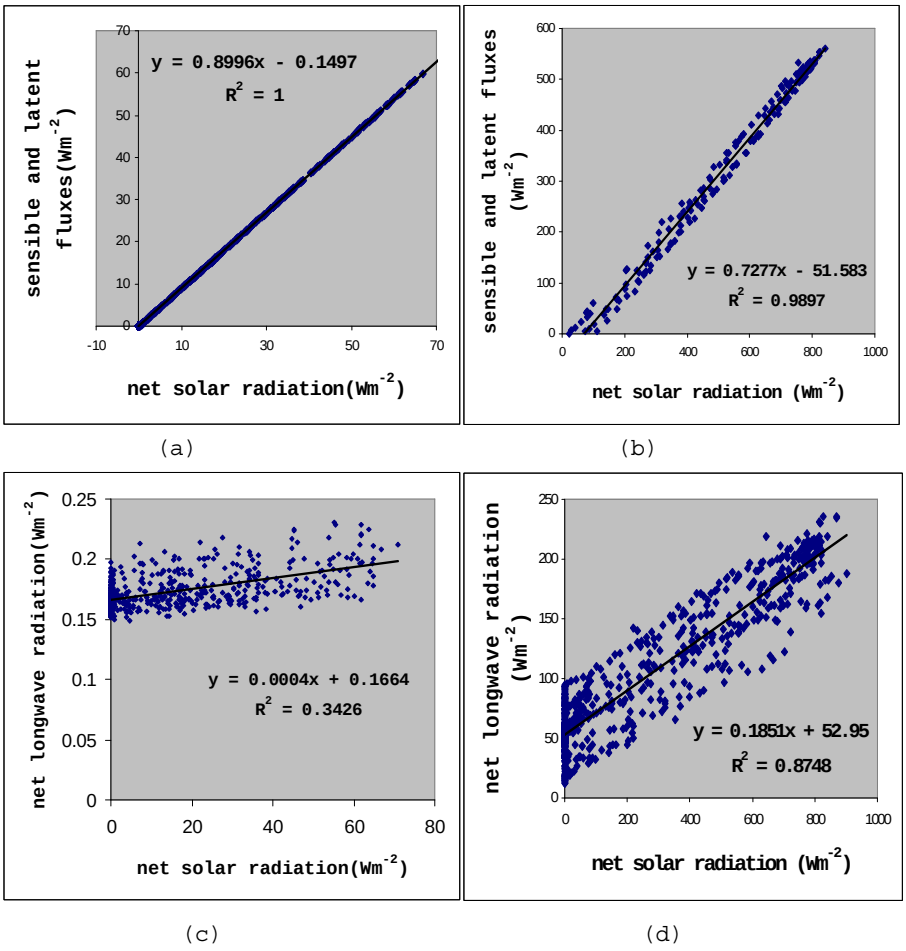

Fig. 3 Correlation between (a)net solar radiation and sensible and latent fluxes in Naivasha;(b)net solar radiation and sensible and latent fluxes in Burkina Faso;(c)net solar radiation and net longwave radiation in Naivasha;(d)net solar radiation and net longwave radiation in Burkina Faso

The LST under clouds was interpolated from the LST of neighboring-pixels temporally or spatially. For the temporal neighboring-pixel interpolation, the LST under clear skies at previous time of the current cloudy pixel was used as reference temperature. Solar radiation of the cloudy pixel minus the solar radiation of pixel without clouds was the difference of solar radiation

between cloudy pixel and pixel under clear skies, namely ΔS_n. For spatial interpolation, the LST under clouds was the average value of interpolated LST under clouds derived from each neighboring pixel within a window of 3×3. The temporal interpolation was implemented if all the neighboring pixels spatially round the center pixel were overcast; otherwise the spatial interpolation was used.

3.6. Hypothesis testing

The t-test was applied to find out if estimates of LST under clear skies, solar irradiance, and LST under clouds were significantly different from the corresponding *in situ* data, respectively.

A linear regression between estimated values and observed values was performed and the optimal fitted trend line was obtained with the approach of least square, which is presented as

$$y=b_1x+b_0 \quad (29)$$

where b_1 is the slope of the optimal trend line, and b_0 is the intercept. In this study, the parameter x was assigned to the estimated values, and y meant the ground-based observations. If $b_1=1$ and $b_0= 0$, it indicates there is no difference between estimated data and *in situ* data.

According to the principle of uncertainty about coefficients of least square, the t-statistics was defined as $\frac{b_1-1}{S_{b1}}$ and $\frac{b_0-0}{S_{b0}}$, respectively, where S_{b1} and S_{b0} were standard deviation of b_1 and b_0.

4. Results

4.1. Results for Ts-clear calculation

The quality of estimated land surface temperature (LST) under clear skies influences the accuracy of estimates LST under clouds. Among many algorithms for LST estimation from satellite observations, the four-channel algorithm was utilized in this research. The brightness temperature products of related channels were input into the model for calculating LST under clear skies. Using the high temporal resolution of SEVIRI data, land surface temperature with time sequence were obtained. Estimated LST of five days without clouds was plotted in Fig. 4. The observed LST was derived from the weather station. For the estimated LST, at the time when the value dropped sharply, it indicates that the pixel was contaminated by clouds.

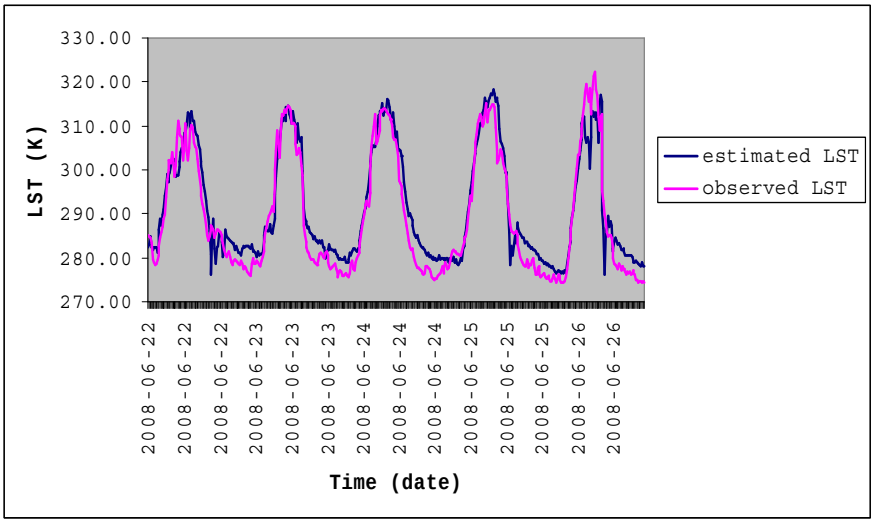

Fig. 4 Comparison between estimated surface temperature in clear sky and observed surface temperature for five days (22nd to 26th June, 2008) in Naivasha

Table 5 Statistical description of estimated LST and observed LST at daytime (22nd to 26th June 2008) in Naivasha

	Estimated LST	Observed LST
Mean (K)	300.66	300.05
Stvd. (K)	11.84	12.13

Table 6 Statistical description of estimated LST and observed LST at nighttime (22nd to 26th June 2008) in Naivasha

	Estimated LST	Observed LST
Mean (K)	282.14	279.24
Stvd. (K)	3.2	3.48

The Fig. 5 shows the comparison between estimated LST and observed LST in daytime and the R-square was 0.8657. For nighttime, the R-square between estimated LST and observed LST was 0.4145 (See Fig. 7). It indicated that the four-channel algorithm had a higher accuracy on estimating LST in daytime than in nighttime. One of the causes is an implementation of solar correction scheme for the middle infrared channel at 3.9 μm in daytime. Against the observed LST in nighttime, the estimated LST from the model had a bias of 2.9 K, and the RMSE was 4.05 K. In daytime, the four-channel algorithm yielded a bias of 0.61 K for estimates of LST, and the RMSE was 4.5 K.

where:

$$RMSE = \sqrt{\frac{\sum_{i=1}^{n}(P_i - Q_i)^2}{n}}$$

$$Bias = \frac{\sum_{i=1}^{n}(P_i - Q_i)}{n}$$

P_i is the estimated value, Q_i is the observed value, n is the number of samples and i is the sample i. Therefore, the four-channel algorithm overestimated LST under clear skies. The RMSE of estimated LST in daytime was greater than that in nighttime (4.5 K versus 4.05 K), and the R-square derived from daytime was also higher than nighttime (0.8657 versus 0.4145). This was caused by the greater variation of LST in daytime.

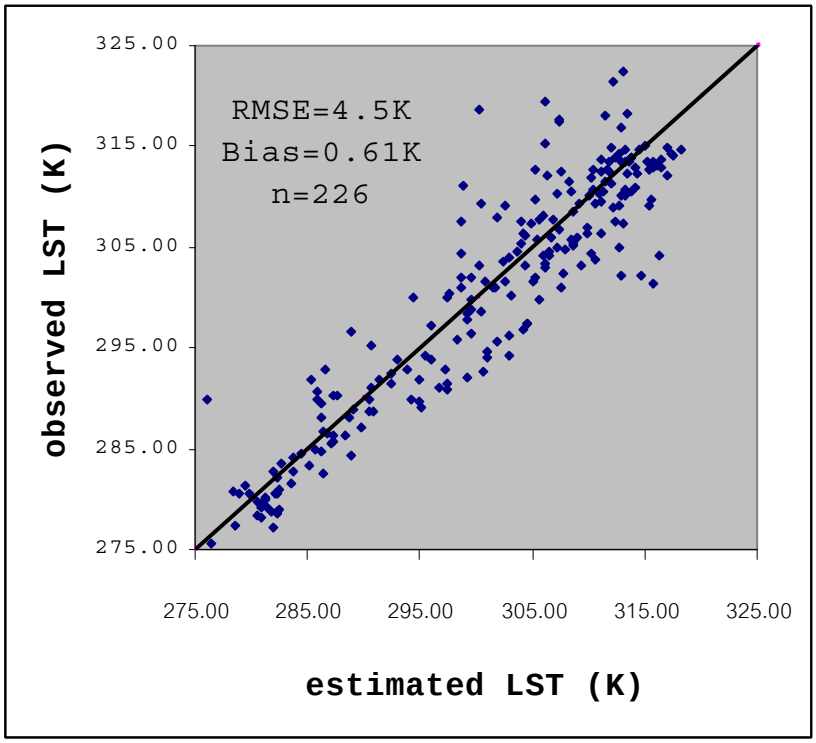

Fig. 5 Estimated LST against observed LST under clear skies at daytime (R^2=0.8657) in Naivasha (the line is 1:1 line)

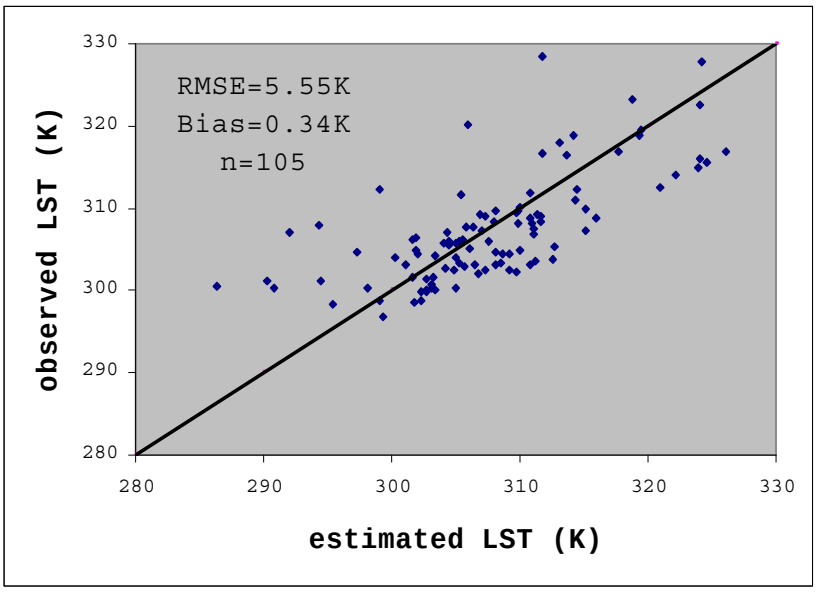

Fig. 6 Estimated LST against observed LST in clear skies at daytime (R^2=0.4982) in Burkina Faso (the line is 1:1 line)

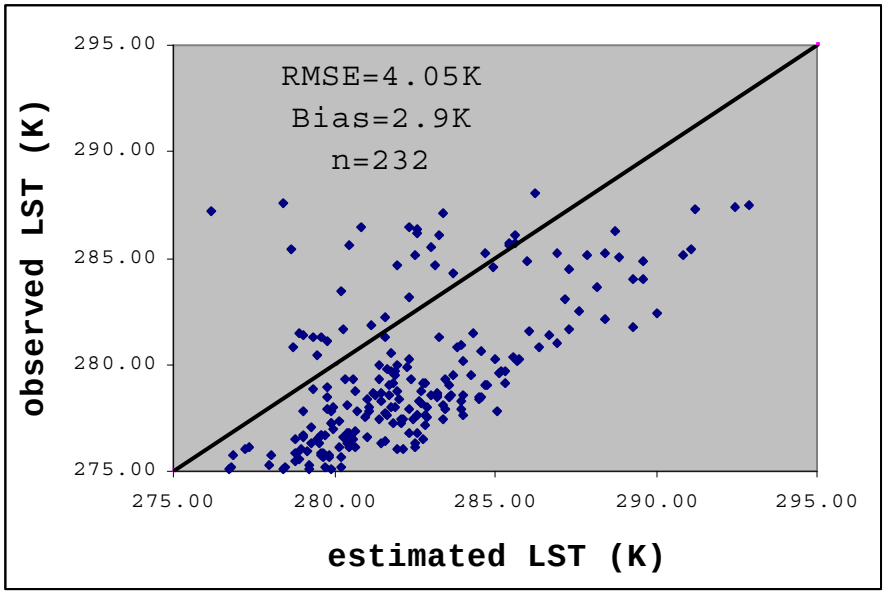

Fig. 7 Estimated LST against observed LST in clear skies at nighttime (R^2=0.4145) in Naivasha (the line is 1:1 line)

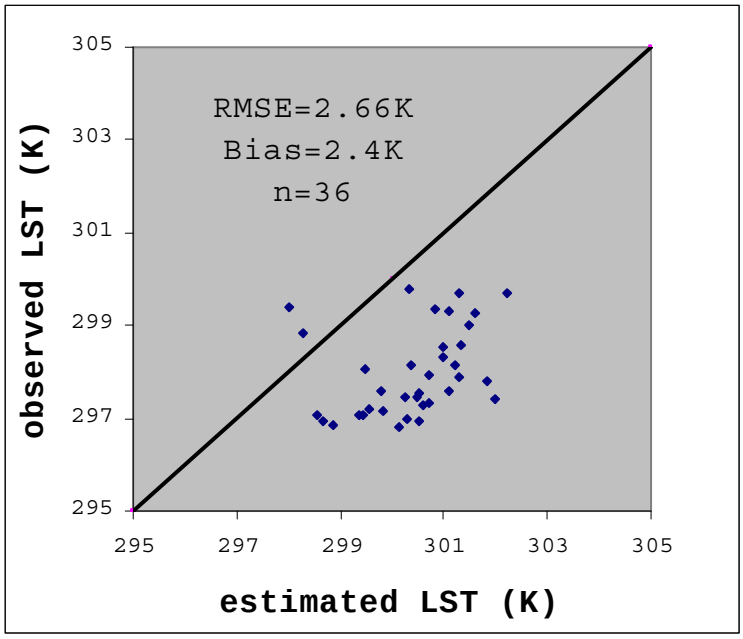

Fig. 8 Estimated LST against observed LST in clear skies at nighttime (R^2=0.1094) in Burkina Faso (the line is 1:1 line)

4.2. Influence of clouds on the estimation of surface temperature (LST)

The statistic analysis on *in situ* data which were categorized into LST under clear skies in daytime and nighttime, LST under clouds in daytime and nighttime indicated the influence of clouds on LST (See Fig. 9). In daytime, LST under clear skies was higher than LST under clouds; the opposite situation occurred in nighttime. This was also demonstrated by ANOVA (Analysis of Variance). In Table 7, the Sig. of interaction between factors named weather and day_night was less than 0.05. This meant there was some interaction between these factors. Therefore, it was not proper to analyze single factor separately. An alternative approach to analyze the influence of two factors on LST is shown as Table 8. It indicated that LST under clear skies was greater than LST under clouds in daytime, and less than LST under

clouds in nighttime due to the interaction between weather conditions (clear skies or with clouds) and time of a day (daytime or nighttime).

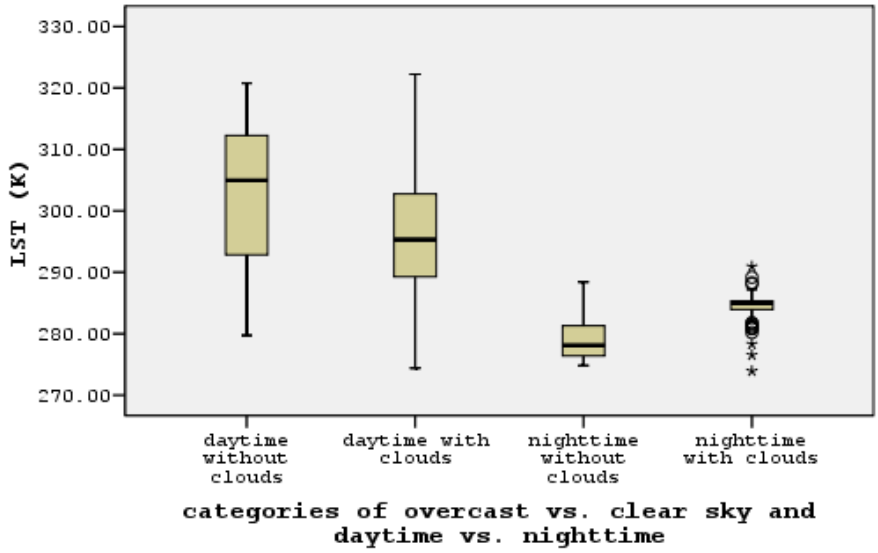

Fig. 9 Influence of clouds on LST in both daytime and nighttime

Table 7 ANOVA analysis on influence of clouds and day-night on LST

Source	Type III Sum of Squares	df	Mean Square	F	Sig.
Corrected Model	34019.532(a)	3	11339.844	264.475	<0.05
Intercept	19732269.076	1	19732269.076	460208.102	<0.05
weather	1018.589	1	1018.589	23.756	<0.05
day_night	30389.680	1	30389.680	708.767	<0.05
weather * day_night	2611.264	1	2611.264	60.901	<0.05
Error	9775.919	228	42.877		
Total	19776064.528	232			
Corrected Total	43795.452	231			

a R Squared = .777 (Adjusted R Squared = .774)

Table 8 Sample mean of treatments (Temperature: Kelvin)

	Day	Night	Row mean
Cloudy skies	297.63	281.45	289.54
Clear skies	308.53	278.93	293.73
Column mean	303.08	280.19	

4.3. Results for solar irradiance estimation

The Heliosat-2 algorithm was utilized to estimate solar irradiance. The R-square value of estimated solar irradiance from satellite observations against observed solar irradiance from the weather station in Naivasha was 0.6227. Table 9 shows statistical description of solar irradiance derived from Heliosat-2 and observed solar irradiance based on data from Naivasha. The standard deviation of solar irradiance was around 300 Wm^{-2}, in which the variation of clouds was likely to be one of the causes. The bias of solar irradiance yielded by Heliosat-2 was 97.74 Wm^{-2}, and the RMSE was 234.05 Wm^{-2}. In Burkina Faso, the bias of estimated solar irradiance was 20.53 Wm^{-2}, and the RMSE was 388.414 Wm^{-2}.

Table 9 Statistical description of solar irradiance estimated from satellite observations and observed solar irradiance in Naivasha (from 22nd to 26th June 2008)

	Estimated solar irridicance	Observed solar irridiance
Mean (Wm^{-2})	607.027	512.28
Standard deviation (Wm^{-2})	348	292.45

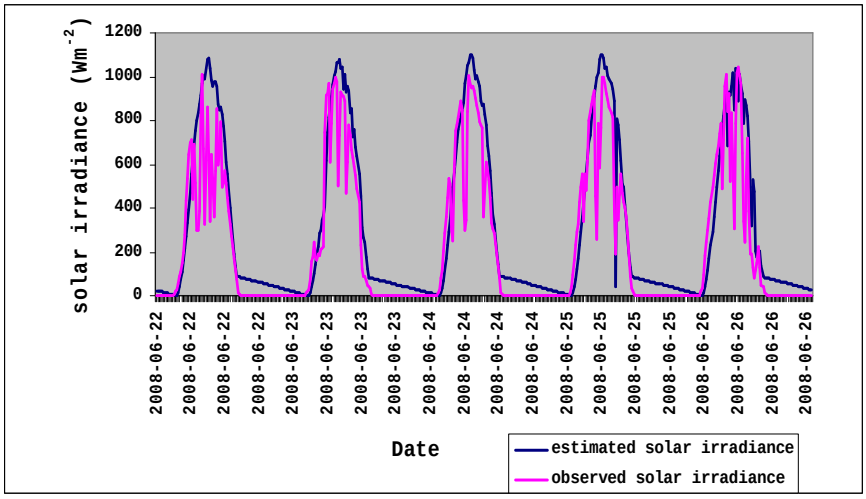

Fig. 10 Comparison of solar irradiance estimated from satellite observations and observed solar irradiance in Naivasha (from 22nd to 26th June 2008)

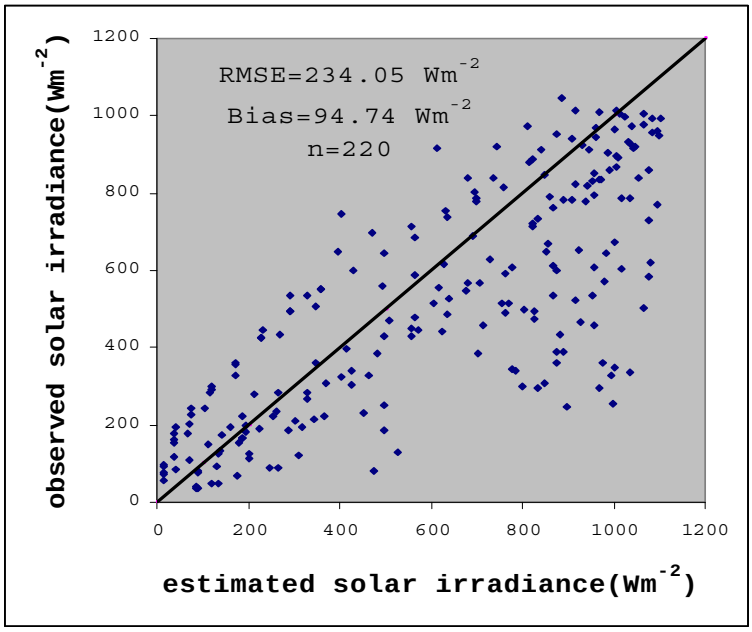

Fig. 11 Estimated solar irradiation against observed solar irradiation in June 2008 in Naivasha (R^2=0.6227) (the line is 1:1 line)

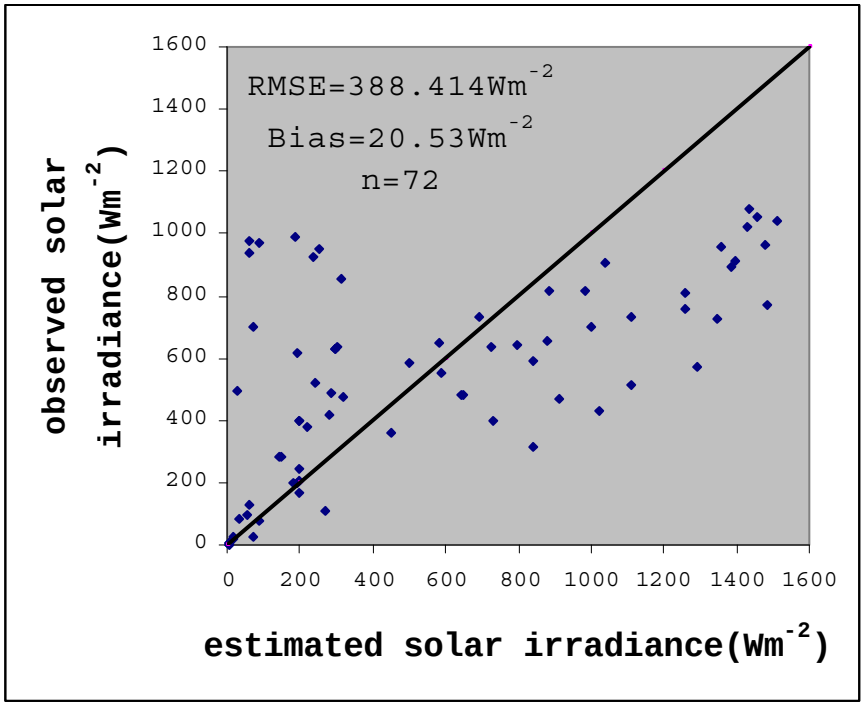

Fig. 12 Estimated solar irradiation against observed solar irradiation in September 2005 in Burkina Faso (R^2=0.3902) (the line is 1:1 line)

4.4. Results for estimation of LST under clouds

Combining the results of LST under clear skies and solar irradiation, LST of cloudy pixels was retrieved by using the neighboring-pixel approach based on SEB. LST under clouds can be interpolated both temporally and spatially. Therefore, LST under clouds was estimated with temporal interpolation. The influence of clouds on LST in 4.2 indicated that the LST of pixels without clouds is greater than the one of cloudy pixels during daytime. Therefore, the difference of solar radiation ΔS_n equals solar radiation of the pixel during cloudy time minus solar radiation of the same pixel under clear skies. If the spatial interpolation is used, ΔS_n should be the solar radiation of pixels under clouds minus solar radiation of their neighboring pixels without clouds at the same time. Fig. 13 shows the LST

under clouds derived from the temporal interpolation against the ground-based observations in Naivasha. Table 10 is a summary of accuracy of estimated LST under clouds derived from different strategies for interpolation with neighboring-pixel approach. The combined interpolation is the strategy of the combination of temporal interpolation and spatial interpolation. The temporal interpolation is used if all neighboring pixels are overcast; otherwise the spatial interpolation is used. Comparing the parameters summarised in Table 10, the temporal interpolation has the highest accuracy in terms of RMSE and Bias.

Table 10 Accuracy of different strategies for interpolation about LST under clouds in Naivasha

	Temporal interpolation	Spatial interpolation	Combined interpolation
R-square	0.5143	0.6954	0.3785
RMSE (K)	5.6	20.14	11.76
Bias (K)	-4	-19.57	-7.23
n	103	27	130

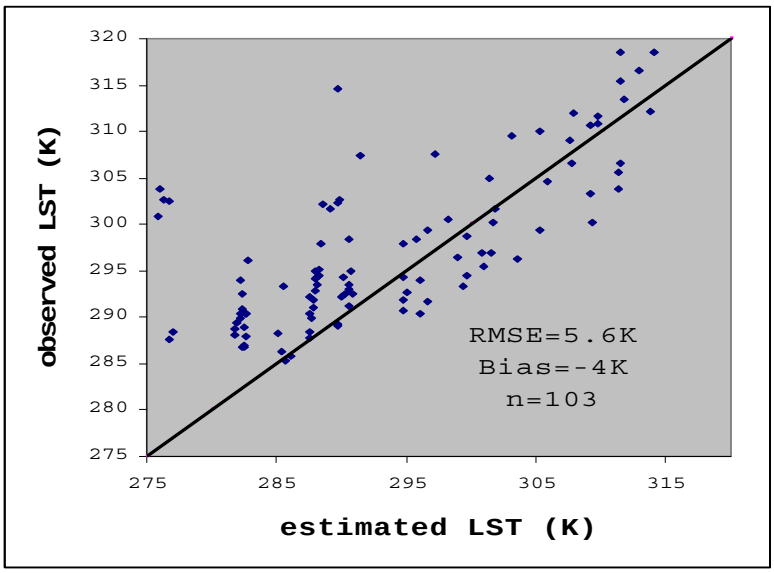

Fig. 13 Estimated LST under clouds with temporal interpolation against observed LST under clouds in Naivasha (R^2=0.5143) (the line is 1:1 line)

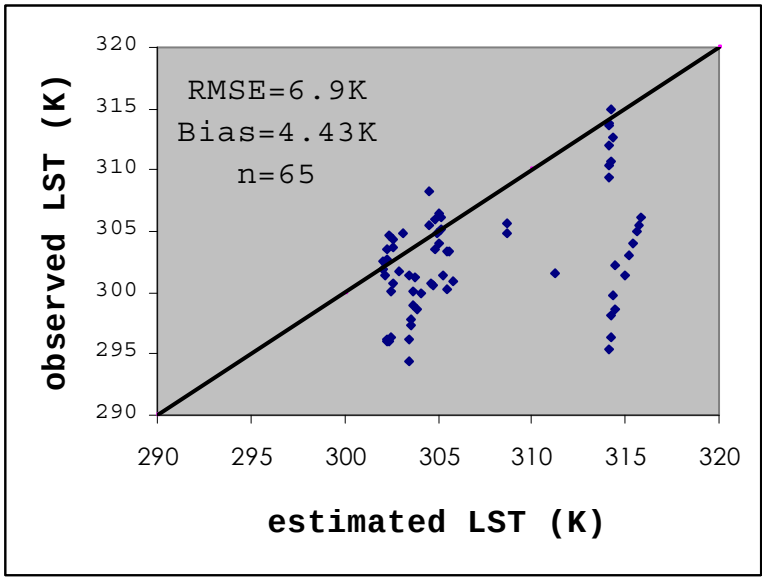

Fig. 14 Estimated LST under clouds with temporal interpolation against observed LST under clouds in Burkina Faso (R^2=0.1791) (the line is 1:1 line)

4.5. Hypothesis testing

The hypotheses were tested on data from Naivasha, Kenya.

(a) For four-channel algorithm to retrieve the LST under clear skies

H_0: There is no difference between estimated LST from the four-channel algorithm and observed LST (b_1=1 and b_0= 0)

Ha: There is difference between estimated LST from the four-channel algorithm and observed LST ($b_1 \neq 1$ and $b_0 \neq 0$)

where b_1 stands for slople, b_0 stands for intercept

Table 11 Statistic description of regression between estimated and observed LST under clear skies (R^2=0.8657 for daytime, R^2=0.4145 for nighttime)

	Coefficient	Standard error
Intercept (daytime)	13.54	7.55
Slope (daytime)	0.95	0.025
Intercept (nighttime)	81.23	15.52
Slope (nighttime)	0.7	0.05

Table 12 Parameters used for hypothesis testing for LST under clear skies (df. = 224 for daytime, df. = 230 for nighttime)

	$b_i \pm$ s.e	t-statistics	P-value
Intercept(daytime)	13.54 ± 7.55	1.7937	<0.1

Slope (daytime)	0.95 ± 0.025	-1.8765	<0.1
Intercept (nighttime)	81.23 ± 15.52	5.2347	<0.05
Slope (nighttime)	0.7 ± 0.05	-5.4222	<0.05

In Table 12, the P-values of both intercept and slope were less than 0.1 in daytime and less than 0.05 in nighttime. Therefore, the hypothesis b_1=1 as well as b_0= 0 were rejected at the level of 0.1. In other words, the null hypothesis "There is no difference between estimated LST from the four-channel algorithm and observed LST" was rejected at the level of 0.1.

(b) For Heliosat-2 algorithm to estimate solar irradiance

H_0: There is no difference between estimated solar irradiance from Heliosat-2 and observed solar irradiance (b_1=1 and b_0= 0)

Ha: There is difference between estimated solar irradiance from Heliosat-2 and observed solar irradiance ($b_1 \neq 1$ and $b_0 \neq 0$)

where b_1 stands for slople, b_0 stands for intercept

Table 13 Statistic description of regression between estimated and observed solar irradiance (R^2=0.6227)

	Coefficient	Standard error
Intercept	109.736	24.45
Slope	0.66	0.035

Table 14 Parameters used for hypothesis testing for solar irradiance (df. = 218)

	bi ± s.e	t-statistics	P-value
Intercept	109.736 ± 24.45	4.49	<0.05
Slope	0.66 ± 0.035	-9.64	<0.05

In Table 14, the P-values of both intercept and slope were less than 0.05. Therefore, the null hypothesis "There is no difference between estimated solar irradiance from Heliosat-2 and observed solar irradiance" was rejected at level of 0.05.

(c) For LST under clouds derived from the method proposed in this research

H_0: There is no difference between estimated LST under clouds and observed LST under clouds

Ha: There is difference between estimated LST under clouds and observed LST under clouds

where b_1 stands for slople, b_0 stands for intercept

Table 15 Statistic description of regression between estimated and observed LST under clouds (R^2=0.5143)

	Coefficient	Standard error
Intercept	128.08	16.38
Slope	0.577	0.056

Table 16 Parameters used for hypothesis testing for LST under clouds (df. = 101)

	bi ± s.e	t-statistics	P-value
Intercept	128.08 ± 16.38	7.8205	<0.05
Slope	0.577 ± 0.056	-7.581	<0.05

In Table 16, the P-values of both intercept and slope were less than 0.05. Therefore, the null hypothesis "There is no difference between estimated LST under clouds and observed LST under clouds" was rejected at the level of 0.05

5. Discussion

The four-channel algorithm overestimates the LST under clear skies. The results for LST under clear skies derived from the four-channel algorithm show an accuracy of 4.5 K for Naivasha, 5.55K for Burkina Faso in daytime. At present, net solar radiation S_n is calculated as incoming solar radiation $S\downarrow$ from the reflected solar radiation at the top of atmosphere (TOA) during which radiative transfer models are usually used and $S\downarrow$ is treated as a function of precipitable water, cloud conditions and solar zenith angle (Pinker and Ewing, 1985; Li et al., 1993). Currently, the accuracy for estimating solar radiation is about 10 Wm^{-2} for monthly mean and 30 Wm^{-2} or more at daily pixel resolution (Jin, 2000). Results of solar irradiance in this study indicated an average error of 234.05 Wm^{-2} yielded by Heliosat-2 algorithm for Naivasha. However, this only contributes 0.82K (234.05 divided by 286 which is the value of K in equ. (15)) to the error of estimated LST under clouds (RMSE=5.6 K for temporal interpolation) in Naivasha. For Burkina Faso, this is a contribution of 2.87 K to the error of estimated LST under clouds (RMSE = 6.9 K for temporal interpolation). Therefore, the error of estimates of LST under clouds is sensitive to the accuracy of estimates of LST under clear skies derived from four-channel algorithm.

Against the ground-based observations, LST under clouds interpolated temporally is more accurate compared with spatial interpolation and combined interpolation. An assumption of the method for estimating LST under clouds is homogeneity of the land surface, so difference of LST between cloudy pixels and clear sky pixels is caused only by occurrence of clouds. In other words, spatial interpolation can not be satisfied using the homogeneity assumption due to the spatial resolution of SEVIRI data. Therefore, to some extent, temporal interpolation eliminated the errors derived from the heterogeneity of land surface, and indicated the validity of

the neighboring-pixel approach based on SEB for retrieval of LST under clouds. Jin (2000) applied this method to polar-orbiting satellite observations, and an accuracy of 1-2 K at monthly mean pixel level resolution was obtained. The temporal interpolation in this study presented an accuracy of 5.6 K at diurnal pixel level resolution in Naivasha, Kenya. In Burkina Faso, the RMSE of estimated LST under clouds against the *in situ* data was 6.9 K. The accuracy of estimated LST under clouds in both Naivasha and Burkina Faso exceeds the range obtained in Jin's (2000) research. One of the reasons is the scale problem between satellite data and *in situ* data during the validation. The *in situ* data came from only one point; however, the spatial resolution of SEVIRI is 3 km. The LST and solar irradiance derived from satellite data are the average values within a pixel with an area of 3×3 km^2. Data from one point on the ground can not represent the values of an area. To improve the accuracy of validation, more samples at the pixel scale on the ground are necessary, and the average value within an area can be interpolated by using these samples.

In addition, ground-based observations of only one point (from the weather station) limit this study to a temporal validation of the results. Though the resolution of thermal bands of SEVIRI data is 3km and 1km for the HRV band, and the land cover data used in four-channel algorithm derived from AVHRR 8km at global scale as well, the consistency of spatial resolution of satellite observations has little influence on the procedure to calculate the final results. For spatial validation, over 30 samples have to be applied which indicates at least 30 points are needed. Additionally, the land cover data with spatial resolution of 1km can be used; and both land cover data and the HRV data of SEVIRI need to be resampled into a resolution of 3km.

In this study, rainfall events were not taken into account. Soil moisture has a significant effect on retrieval of LST via its impact on emissivity. For modeling the diurnal cycle of LST, soil moisture influences its amplitude and the lag in LST maxima. It has been demonstrated empirically (Sun and Pinker, 2004) that errors of LST derived from satellite measurements increase with the decrease of soil moisture. However, in the four-channel algorithm used in this study, the surface emissivity was calculated according

to a linear mixing with weighted sum of land cover percentage times the emissivity of corresponding surface type, the effect of rainfall was not taken into account.

The attenuation of haze in visible bands is more than the reduction of infrared radiation because of the smallness of its particles as mentioned in Chapter 2. In this study, discrimination between clouds and haze was not referred to, and only clouds were assumed occurring in the study area.

The neighboring-pixel approach based on SEB interpolates the surface temperature under clouds with the land surface temperature derived from clear sky conditions and the difference of net solar radiation between cloudiness and clear skies. In terms of the Heliosat-2 algorithm for estimating solar radiation, the cloud detection utilized the threshold approach, and solar radiation under clouds was estimated by the parameter of cloud index. Both of the two processes assumed that the count of cloudy pixels would be brighter than the one for pixels without clouds. The top of the clouds reflects solar radiation strongly. However, cirrus clouds have low solar reflectivities and low emissivities (Liou, 1986). Therefore, unlike most other clouds, cirrus can increase the net radiative heating of the earth if they are optically thin enough; if they are thicker, the decrease of the net radiative heating is still the dominant effect on the radiative balance. Thus, the method for estimating surface temperature under clouds used in this research is not suitable for the cirrus condition.

Using geo-stationary satellite observations, LST of all skies (under both clear skies and cloudy skies) at hourly scale can be retrieved with the neighboring-pixel approach based on SEB. However, for this method, LST under clouds was interpolated from LST of neighboring-pixel under clear skies and the difference of net solar radiation between cloudy pixel and pixels without clouds, which indicates that solar radiation is indispensable. Therefore, LST under clouds at night time can not be obtained with this method. To obtain diurnal LST in all skies, new method to estimate LST under clouds at night time has to be developed.

Finally, the results of LST under clouds derived from different interpolate strategies indicate that this method would be applied at a global scale or large regional scale to obtain the information of LST in all skies with high temporal resolution, so that further understanding of mechanism of interaction between clouds and LST as well as climatic studies can be achieved.

6. Conclusions and Recommendations

6.1. Conclusions

The general objective of this study for estimating LST under clouds by using geo-stationary satellite observations was achieved with the neighboring-pixel approach based on SEB.

The accuracy of the four-channel algorithm to estimate LST under clear skies is 4.5 K for Naivasha and 5.55 K for Burkina Faso in daytime, and 4.05 K for Naivasha and 2.66 K for Burkina Faso in nighttime. It contributes large parts to the error of estimates of LST under clouds.

Heliosat-2 algorithm yielded an accuray of 234.05 Wm^{-2} of estimated solar irradiance for Naivasha, and 388.414 Wm^{-2} for Burkina Faso.

For the neighboring-pixel approach, three interpolation strategies were explored in Naivasha, and the temporal interpolation (RMSE=5.6 K) has the best accuracy against spatial interpolation (RMSE=20.14K) and combined interpolation (RMSE=11.76 K). Using the temporal interpolation, the RMSE of estimating LST under clouds is 6.9 K in Burkina Faso.

The null hypothesis, that there is no difference between LST under clouds derived from the geo-stationary satellite observations and LST derived from ground-based data, was rejected at the level of 0.05.

6.2. Recommendations

For further research, the following suggestions are recommended:
The conclusion shows good agreement between the estimated and observed LST under clouds by applying the neighboring-pixel approach to geo-stationary satellite data under the combination of four-channel algorithm and

Heliosat-2 algorithm. However, this method can be only utilized for daytime, to obtain the diurnal LST in all skies, method for estimating LST under clouds at nighttime is compulsory to be developed.

The method applied to geo-stationary satellite data is validated temporally due to lack of enough spatial samples for statistic analysis. For further robust evidence of this application, more than 30 spatial samples are required and spatial validation is necessary. To improve the accuracy of validation, more samples on the ground are needed.

7. Reference

Aires F., Prigent C. and Rossow W.B.. 2004. Temporal interpolation of global surface skin temperature diurnal cycle over land under clear and cloudy conditions. Journal of Geophysical Research 109.

Becker F. and Li Z.L.. 1990. Temperature-independent spectral indices in thermal infrared bands. Remote Sensing of Environment 32: 17-33.

Caselles V., Coll C. and Valor E.. 1997. Land surface emissivity and temperature determination in the whole HAPEX-Sahel area from AVHRR data. International Journal of Remote Sensing 18(5): 1009-1027.

Chameides W.L., Yu H., Liu S.C., Bergin M., Zhou X., Mearns L., Wang G., Kiang C.S., Saylor R.D., Luo C., Huang Y., Steiner A. and Giorgi F.. 1999. Case study of the effects of atmospheric aerosols and regional haze on agriculture: An opportunity to enhance crop yields in China through emission controls? Proceeding of the National Academy of Sciences 96(24): 13626-13633.

Chchbouni A., Njoku E.G., Lhommc J.P. and Kcrr Y.H.. 1993. An approach for averaging surface temperature and surface fluxes over heterogeneous terrain. URL: http://trs-new.jpl.nasa.gov/dspace/simple-search?query=An+approach+for+Averaging+Surface+Tcmpcraturc+and+Surface+Fluxes&submit=Go Access date: 10-Januray-2009

Chen C.C.. 1975. Attenuation of electromagnetic radiation by haze, fog, clouds, and rain. URL: http://wwwcgi.rand.org/pubs/reports/2006/R1694.pdf Access date: 12-November-2008.

Chen L.F., Zhuang J.L., Xu X.R., Niu Z., Zhang R.H. and Xiang Y.Q.. 2000. The concept
of effective emissivity of nonisothermal mixed pixel and its test. Chinese Science Bulletin 45(9):788-795.

Chung C.E., Ramanathan V. and Kiehl J.T.. 2002. Effects of the South Asian absorbing haze on the northeast monsoon and surface-air heat exchange. Journal of Climate 15: 2462-2476.

Coll C., Caselles V., Valor E., Niclòs R., Sánchez J.M., Galve J.M. and Mira M.. 2007. Temperature and emissivity separation from ASTER data for low spectral contrast surfaces. Remote Sensing of Environment 110: 162-175.

Dagestad K.F. and Olseth J.A.. 2005. An alternative algorithm for calculating the cloud index. URL: http://www.nersc.no/~knutfd/documents/phd_thesis/Dagestad_paper3.pdf Access date: 20-September-2008

Dai A.G., Trenberth K.E. and Karl T.R.. 1999. Effects of clouds, soil moisture, precipitation, and water vapor on diurnal temperature range. Journal of Climate 12: 2451-2473.

Dash P., Göttsche F.M. and Olesen F.S.. 2002. Potential of MSG for surface temperature and emissivity estimation: considerations for real-time applications. International Journal of Remote Sensing 23(20): 4511-4518.

Deardorff J.W.. 1978. Efficient prediction of ground surface temperature and moisture, with inclusion of a layer of vegetation. Journal . Geophys. Res., 83:1889–1903,.

Deneke H.M., Feijt A.J. and Roebeling R.A.. 2008. Estimating furface solar irradiance from METEOSAT SEVIRI-derived cloud properties. Remote Sensing of Environment 112(6): 3131-3141.

Dickinson R.E..1988.The force-restore model for surface temperatures and its generalization. Journal of Climate 1: 1086–1097

François C.. 2002. The potential of directional radiometric temperatures for monitoring soil and leaf temperature and soil moisture status. Remote Sensing of Environment 80: 122-133.

Galve J.M., Coll C., Caselles V., Niclòs R., Valor E., Sánchez J.M. and Mira M.. 2007.A cloudless land atmosphere radiosounding database for generating land surface temperature retrieval algorithms. IEEE International 1899-1902.

Goïta K. and Royer A.. 1997. Surface temperature and emissivity separability over land
surface from combined TIR and SWIR AVHRR data. IEEE Transactions on Geoscience
and Remote Sensing 35(3): 718-733.

Göttsche F.M. and Olesen F.S.. 2001. Modelling of diurnal cycles of brightness temperature extracted from METEOSAT data. Remote Sensing of Environment 76: 337-348.

Groisman P.Y., Bardley R.S. and Sun B.M.. 2000. The relationship of cloud cover to near-surface temperature and humidity: Comparison of GCM simulations with empirical
data. Journal of Climate 13: 1858-1878.

Guo X.Y. and Cheng G.D..2004. Remote sensing study of evapotranspiration in the Heihe River Basin, Northwest of China. IEEE International 6: 3607-3610.

Gupta S.K., Darnell W.L. and Wilber A.C.. 1992. A parameterization for longwave surface radiation from satellite data recent improvements. Journal of Applied Meteorology 31(12): 1361-1367.

Heffter C.P., Liu Q., Ruprecht E. and Simmer C.. 1995. Effect of cloud types on the earth radiation budget calculated with the ISCCP C1 dataset: methodology and initial results. Journal of Climate 8: 829-843.

Jacobs J.M., Anderson M.C., Friess L.C. and Diak G.R.. 2004. Solar radiation, longwave radiation and emergent wetland evapotranspiration estimates from satellite data in Florida, USA. Journal of Hydrological Sciences 49(3): 461-476.

Jiménez-Muñoz J.C. and Sobrino J.A.. 2003. A generalized single-channel method for retrieving land surface temperature from remote sensing data. Journal of Geophysical Research 108(D22): 4688-4696.

Jin M.L.. 2000. Interpolation of surface radiative temperature measured from polar orbiting satellites to a diurnal cycle 2. cloudy-pixel treatment. Journal of Geophysical Research 105(D3): 4061-4076.

Jin M.L. and Dickinson R.E.. 2002. New observational evidence for global warming from satellite. Geophysical Research Letters 29(10)

Jin M.L., Dickinson R.E. and Vogelmann A.M.. 1997. A comparison of CCM2-BATS
skin temperature and surface-air temperature with satellite and surface observations.
American Meteorological Society 10: 1505-1524.

Jin Y., Rossow W.B. and Wylie D.P.. 1996. Comparison of the climatologies of high-level clouds from HIRS and ISCCP. Journal of Climate 9: 2850-2879.

Kearney M. and Porter W.P.. 2004. Mapping the fundamental niche: physiology, climate, and the distribution of a nocturnal lizard. Ecology 85(11): 3119-3131.

Key J.R. and Wong A.M.. 1999. Estimating the cloudy sky surface temperature of sea ice
with optical satellite data. IEEE International 320-322.

Lakshmi V., Susskind J. and Choudhury B.J.. 1998. Determination of land surface skin temperatures and surface air temperature and humidity from TOVS HIRS2/MSU data. Advances in Space Research 22(5): 629-636.

Lefèvre M., Albuisson M. and Wald L.. 2002. Description of the software Heliosat-Π for the conversion of images acquired by Meteosat satellites in the visible band into maps of solar radiation available at ground level. URL: http://www.helioclim.net/heliosat/heliosat2_soft_descr.pdf Access date: 10-Octomber-2008

Li Z., Leighton H.G., Masuda K. and Takashima T.. 1993. Estimation of SW flux absorbed at the surface from TOA reflected flux. Journal of Climate. 6: 317–330.

Lim A., Liew S.C. and Kwoh L.K.. 2004. Retrieval of land surface temperature in the humid tropics from MODIS data by modeling the atmospheric transmission and thermal emission. Proc. 2004 IEEE International Geoscience and Remote Symposium, September 20-24, 2004, Anchorage, Alaska, USA

Liou K.N.. 1986. Influence of cirrus clouds on weather and climate processes: a global perspective. Monthly Weather Review, 114(6): 1167-1199.

Mallick K., Bhattacharya B.K., Chaurasia S., Dutta S., Nigam R., Mukherjee J., Banerjee S., Kar G., Rao V.U.M., Gadgil A.S. and Parihar J.S.. 2007. Evapotranspiration using MODIS data and limited ground observations over selected agroecosystems in India. International Journal of Remote Sensing 28(10): 2091-2110.

McNider R.T., Song A.J., Casey D.M., Wetzel P.J., Crosson W.L. and Rabin R.M.. 1994. Toward a dynamic-thermodynamic assimilation of satellite surface temperature in numerical atmospheric models. Monthly Weather Review 122: 2784-2803

Minnis P. and Harrison E.F.. 1984. Diurnal variability of regional cloud and clear-sky radiative parameters derived from GOES data. Part I: Analysis method. Journal of Climate and Applied Meteorology 23(7): 993-1011.

Minnis P., Heck P.W., and Harrison E.F.. 1990. The 27-28 October 1986 FIRE IFO Cirrus Case Study: Cloudy parameter fields derived from satellite data.Monthly Weather Review 118:2426-2447.

Minns P. and Khaiyer M.M.. 2000. Anisotropy of land surface skin temperature derived from satellite data. Journal of Applied Meteorology 39: 1117-1129.

Nandagiri L. and Kovoor G.M.. 2005. Sensitivity of the Food and Agriculture Organization Penman-Monteith evapotranspiration estimates to alternative procedures for estimation of parameters. Journal of Irrigation and Drainage Engineering, 131(3): 238-248

Paltridge G.W..1974. Global cloud cover and earth surface temperature. Journal of The
Atmospheric Sciences 31: 1571-1576.

Peters-Lidard C.D., Blackburn E., Liang X. and Wood E.F.. 1998. The effect of soil thermal conductivity parameterization on surface energy fluxes and temperatures. Journal of the Atmospheric Sciences 55: 1209-1224.

Peres L.F. and DaCamara C.C.. 2004. Land surface temperature and emissivity estimation based on the two-temperature method: sensitivity analysis using simulated MSG/SEVIRI data. Remote Sensing of Environment 91: 377-389.

Peres L.F. and DaCamara C.C.. 2005. Emissivity maps to retrieve Land-Surface Temperature from MSG/SEVIRI. IEEE Transaction on Geoscience and Remote Sensing 43(8): 1834-1844.

Peres L.F. and DaCamara C.C.. 2006. Improving two-temperature method retrievals based on a nonlinear optimization approach. IEEE Geoscience and Remote Sensing Letters 3(2): 232-236.

Pinker R.F. and Ewing J.A.. 1985. Modeling surface solar radiation: Model formulation and validation. Journal of Applied Meteorology 24(5):389–401.

Qin Z., Karnieli A. and Berliner P.. 2001. A mono-window algorithm for retrieving land surface temperature from Landsat TM data and its application to the Israel-Egypt border region. International Journal of Remote Sensing 22(18): 3719-3746.

Rossow W.B., Mosher F., Kinsella E., Arking A., Desbois M., Harrison E., Minnis P., Ruprecht E., Seze G., Simmer C. and Smith E.. 1985. ISCCP cloud algorithm intercomparison. Journal of Climate and Applied Meteorology 24(9): 877-903.

Schneider S.H., Washington W.M. and Chervin R.M.. 1978. Cloudiness as a climatic feedback mechanism: effects on cloud amounts of prescribed global and regional surface temperature changes in the NCAR GCM. Journal of the Atmospheric Science 35(12): 2207-2221.

Smith G.L., Wielicki B.A., Barkstrom B.R., Lee R.B., Priestley K.J., Charlock T.P., Minnis P., Kratz D.P., Loeb N. and Young D.F.. 2004. Clouds and earth radiant energy system: an overview. Advances in Space Research 33: 1125-1131.

Sobrino J.A., Jiménez-Muñoz J.C. and Paolini L.. 2004. Land surface temperature retrieval from LANDSAT TM 5. Remote Sensing of Environment 90: 434-440.

Sobrino J.A., Li Z.L., Stoll M.P. and Becker F.. 1994. Improvements in the split-window technique for land surface temperature determination. IEEE Transaction on Geoscience and Remote Sensing 32(2): 243-253.

Stisen S., Sandholt I., Nørgaard A., Fensholt R. and Eklundh L.. 2007. Estimation of diurnal air temperature using MSG SEVIRI data in west Africa. Remote Sensing of Environment 110: 262-274.

Sun D.L. and Pinker R.T.. 2004. Case study of soil moisture effect on land surface temperature retrieval. IEEE Geoscience and Remote Sensing Letters 1(2): 127-130.

Sun, D., and R. T. Pinker (2007), Surface temperature retrieval from MSGSEVIRI observations, Int. J. Remote Sens, in press.

Timmermans J., Tol C.V.D., Verhoef W. and Su Z.. 2008. Contact and directional radiative temperature measurements of sunlit and shaded land surface components during the SEN2FLEX 2005 campaign. International Journal of Remote Sensing 29(17-18): 5183-5192.

Ulivieri C., Castronuovo M.M., Francioni R. and Cardillo A.. 1994. A split window algorithm for estimating land surface temperature from satellites. Advances in Space Research 14(3): 359-365.

Valor E., Coll C., Caselles V. and Niclòs R.. 2003. The adjusted normalized emissivity method (ANEM) for land surface temperature and emissivity recovery. Geoscience and Remote Sensing Symposium, 2003. 5: 3088-3090.

Venus V. and Rugege D.. Combined use of polar orbiting and geo-sationary satellites to improve time interpolation in dynamic crop models for food security assessment. URL: http://www.cartesia.org/geodoc/isprs2004/comm7/papers/41.pdf Access date: 10-November-2008

Wang L., Qu J.J., Zhang S., Hao X. and Dasgupta S.. 2007. Soil moisture estimation using MODIS and ground measurements in eastern China. International Journal of Remote Sensing 28(6): 1413-1418.

Yang H. and Yang Z.D.. 2006. A modified land surface temperature split window retrieval algorithm and its applications over China. Global and Planetary Change 52: 207-215.

Yao J., Rossow W.B. and Wylie D.P.. 1996. Comparison of the climatologies of high-level clouds from HIRS and ISCCP. Journal of Climate 9: 2850-2879.

Zhang W.C., Zhu Y.F. and Xu S.J.. 2007. Mono-window algorithm for retrieval of land surface net long-wave radiation in mountainous area. IEEE International 1680-1684.

http://www.eumetsat.int/Home/Main/Access_to_Data/Meteosat_Image_Services/SP_1123237865326 Access date: 20-Octomber-2008

8. Appendix

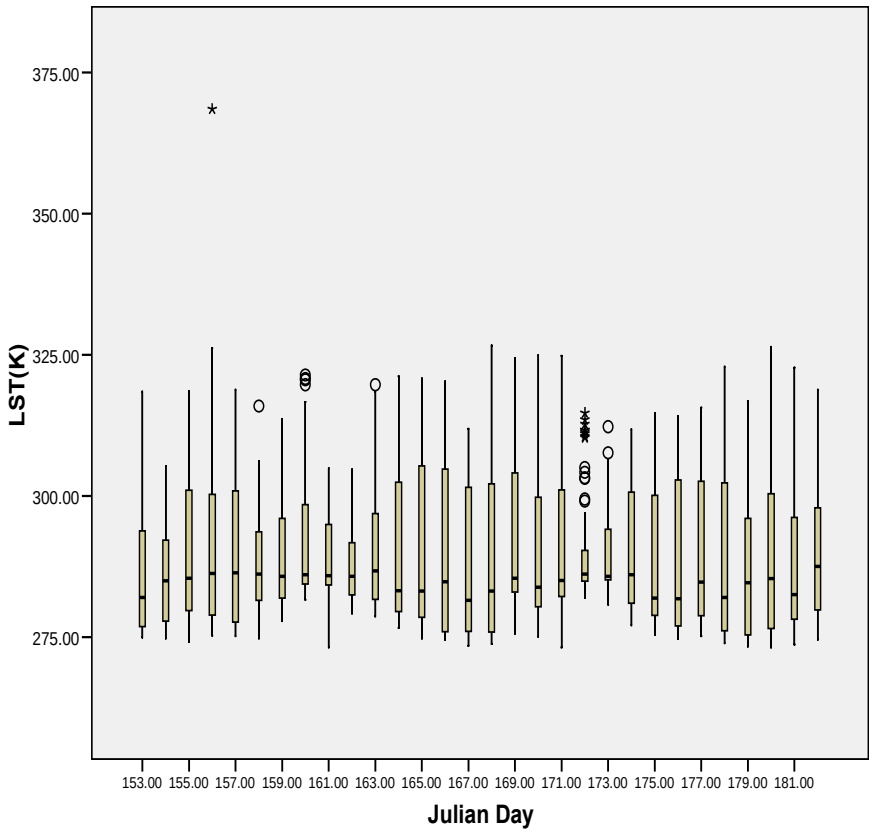

APP.Fig 1 Statistic description of daily LST in June 2008 in Naivasha

From this graph, it can be set that the diurnal LST in June should range from 275 K to 325 K.

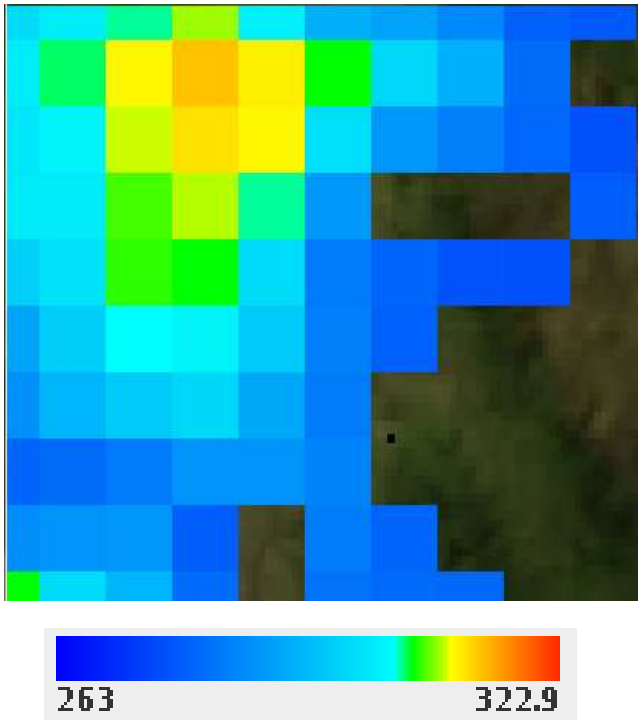

APP.Fig 2 Image of estimated LST (2008/06/22 11:15:00 UTC, the unit of LST is Kelvin) (The pixels with missing value are overcast) Influence of clouds on the estimation of land surface temperature (LST)